European Journal of Medicinal Chemistry 283 (2025) 117102

Contents lists available at ScienceDirect

European Journal of Medicinal Chemistry

journal homepage: www.elsevier.com/locate/ejmech

Research paper

# Chemical probes for the identification of the molecular targets of honokiol

Henar Vázquez-Villa [a,1], Ainoa Rueda-Zubiaurre [a,1], Daniel Fernández [a], Román Foronda [a], Christopher G. Parker [b], Benjamin F. Cravatt [b], Mar Martín-Fontecha [c,**], Silvia Ortega-Gutiérrez [a,*]

[a] Departamento de Química Orgánica, Facultad de Ciencias Químicas, Plaza de las Ciencias s/n, Universidad Complutense de Madrid, E-28040, Madrid, Spain
[b] Department of Chemistry, Scripps Research, La Jolla, CA, 92037, United States
[c] Departamento de Química Orgánica, Facultad de Óptica y Optometría, Avda. Arcos de Jalón, 118, Universidad Complutense de Madrid, E-28037, Madrid, Spain

ARTICLE INFO

*Keywords:*
Honokiol
Target identification
Chemical probes
Chemical proteomics
Photoaffinity labeling

ABSTRACT

Honokiol is a natural product with an interesting array of biological effects, including significant anti-tumor properties. However, full exploration of its therapeutic potential is hampered by its modest pharmacokinetic profile and by the lack of synthetic methods that allow to obtain specifically designed derivatives with improved properties. In addition, the specific molecular targets of honokiol remain poorly understood, a fact that limits the search of alternative hits for subsequent optimization programs. In this work we describe an optimized series of synthetic routes that allow to access to a variety of honokiol derivatives, including a set of minimalist photoaffinity probes to map potential protein targets in live cells. Chemical proteomic studies of the most potent probe revealed a defined set of proteins as the cellular targets of honokiol. Significantly, up to the 62 % of the identified proteins have described roles in cancer, highlighting their potential relationship with the antitumor effects of honokiol. Furthermore, several of the top hits have been validated as direct binding partners of honokiol by cellular thermal shift assay (CETSA). In sum, the work described herein provides the first landscape of the cellular targets of honokiol in living cells and contributes to define the specific molecular pathways affected by this natural product.

## 1. Introduction

Honokiol (Fig. 1A) is a lignan compound found in the bark of the *Magnolia* plant family. This natural product has shown an interesting array of biological properties, including antiviral, antimicrobial, anxiolytic, anti-tumor and anti-inflammatory effects [1–7]. Among these effects, its potential for inducing cytotoxicity in cellular models of highly resistant cancers such as triple negative breast cancer (TNBC), non-small cell lung cancer (NSCLC), and oral squamous cell carcinoma (OSCC) has garnered much attention [8–13]. However, some limitations hamper an in-depth exploration of honokiol clinical potential, including moderate pharmacokinetic parameters that translate into a low oral bioavailability, and, more important, a lack of knowledge about its specific therapeutic targets. In this context, most studies describe phenotypic assays or cellular pathways that are affected by honokiol, but not the specific interaction partners [5,12,14,15]. Accordingly, identification of honokiol molecular targets still remains an open question whose answer could reveal new therapeutic strategies for addressing important unmet medical needs, including TNBC, NSCLC, and OSCC. Chemical proteomics is one of the most powerful methods to connect a molecule with its interaction partners [16,17]. It relies on the preparation of a chemical probe, a compound that keeps the bioactivity of the parent drug, but that has been modified with a reporter tag to enable the subsequent isolation and identification by mass spectrometry of the compound targets [18], and has been successfully used for establishing the interaction partners of different natural products, endogenous metabolites, and approved or under development drugs including (*R*)-lipoic acid [19], ingenol mebutate [20], portimines [21], catechols [22], 20(*S*)-hydroxycholesterol [23], serotoninergic ligands [24], curcusone diterpenes [25], gamboic acid [26], phloroglucinol meroterpenoids [27], and fructose-1,6-bisphosphate [28] just to mention some recent examples. Application of this approach to honokiol requires the preparation of chemical probes based on the scaffold of the natural product as bioactive

* Corresponding author.
** Corresponding author.
*E-mail addresses:* marmmart@ucm.es (M. Martín-Fontecha), siortega@ucm.es (S. Ortega-Gutiérrez).
[1] Equal contribution.

https://doi.org/10.1016/j.ejmech.2024.117102
Received 1 August 2024; Received in revised form 3 November 2024; Accepted 12 November 2024
Available online 24 November 2024

**Abbreviations**

| | |
|---|---|
| BSA | bovine serum albumin |
| CAPN-1 | calpain-1 |
| CETSA | cellular thermal shift assay |
| CuAAC | copper-catalyzed azide-alkyne cycloaddition |
| DAVID | database for annotation, visualization and integrated discovery |
| DCC | dicyclohexylcarbodiimide |
| DMAP | 4-dimethylaminopyridine |
| DPP3 | dipeptidyl peptidase 3 |
| GO | gene onthology |
| HNSCC | head and neck squamous cell carcinoma |
| HOBt | 1-hydroxybenzotriazole |
| EMT | epithelial-mesenchymal transition |
| ER | estrogen receptor |
| HER2 | human epidermal growth factor 2 |
| MW | microwave |
| OSCC | oral squamous cell carcinoma |
| NSCLC | non-small cell lung cancer |
| PANTHER | protein annotation through evolutionary relationship |
| PGD | 6-phosphogluconate dehydrogenase, decarboxylating |
| PR | progesterone receptor |
| SDS-PAGE | sodium dodecyl-sulfate polyacrylamide gel electrophoresis |
| SILAC | stable isotope labeling by amino acids in cell culture |
| TBTA | tris[(1-benzyl-1*H*-1,2,3-triazol-4-yl)methyl]amine |
| TCEP | tris(2-carboxyethyl)phosphine |
| TFA | trifluoroacetic acid |
| TNBC | triple negative breast cancer |

moiety, but few synthetic methods that enable to access honokiol and its derivatives in a systematic manner have been developed, since many of the studies have been performed with compounds isolated from the natural source or with mixtures of plant active principles. Hence, in this work we describe four optimized synthetic routes that allow to access to a variety of honokiol derivatives. Of note, the synthesized alkyne or azide intermediates can be the starting point for late-stage functionalization through copper-catalyzed azide–alkyne cycloaddition (CuAAC) to expand the number of accessible honokiol derivatives. In this work, these routes have been used to obtain a set of minimalist chemical

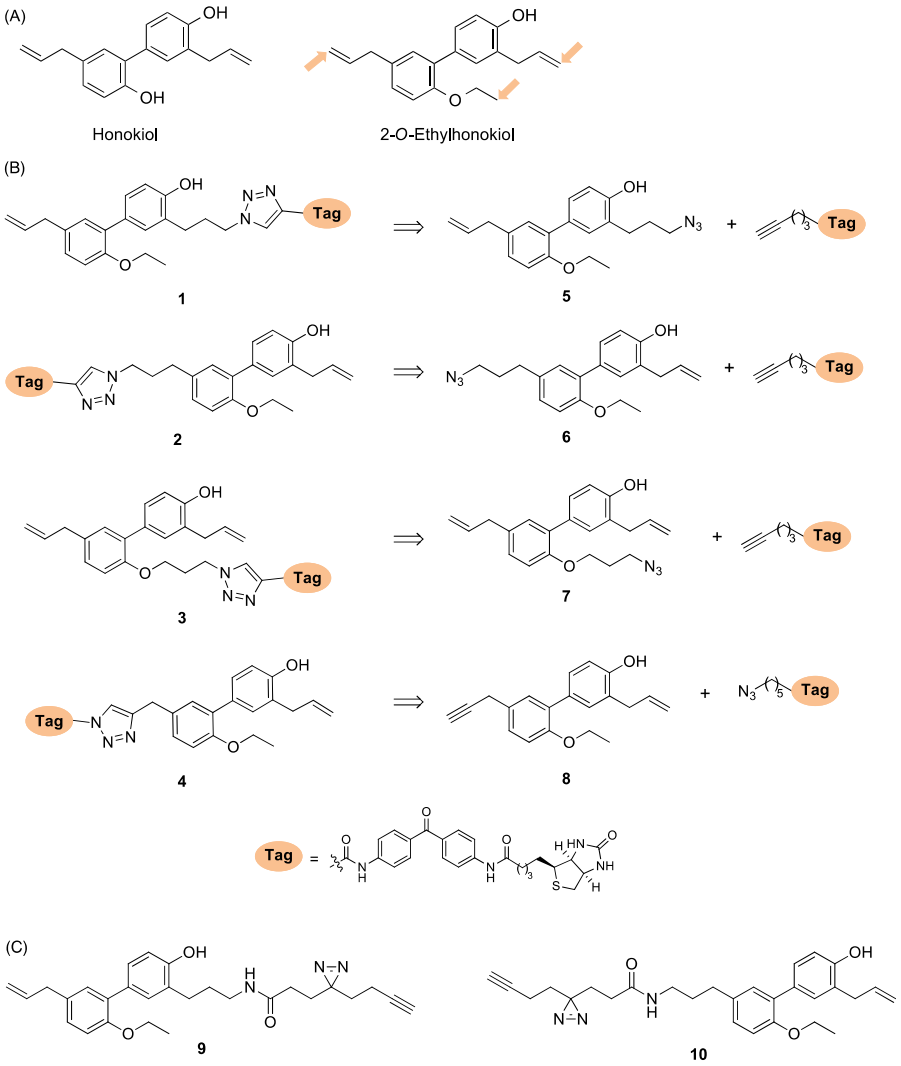


**Fig. 1.** (A) Structures of honokiol and 2-*O*-ethylhonokiol. (B, C) Design of probes **1**–**4**, **9**, and **10**.

probes based on the honokiol scaffold that keep the biological activity of the parent compound and are able to label proteins in living cells in a specific manner. The best probe has been used to perform chemical proteomic experiments in competition with honokiol. These studies have revealed a defined set of proteins as the cellular targets of honokiol. Significantly, up to the 62 % of the identified proteins have been described as involved in cancer, and up to the 50 % of them have been characterized as strongly selective or common essential in the cancer dependency map, highlighting their potential relationship with the antitumor effects of honokiol. Furthermore, some of the top hits have been validated as direct binding partners of honokiol by cellular thermal shift assay (CETSA). All in sum, the work described herein provides the first landscape of the cellular targets of honokiol in living cells and contributes to define the specific molecular pathways affected by this natural product.

## 2. Results and discussion

### 2.1. Probe design

As mentioned above, a chemical probe has three key structural elements: the bioactive subunit that binds to the protein targets, a reporter tag for their isolation and subsequent identification, and a linker that separates the bioactive subunit and the tag to minimize potential steric interferences that could affect binding. As the bioactive subunit, we have selected 2-*O*-ethylhonokiol (Fig. 1A), a slightly modified honokiol analogue that exhibits comparable or even better anti-proliferative properties than honokiol [9,10]. With respect to the tag, we have considered classical biotin and benzophenone-containing moieties but also minimalist tags such as a diazirine combined with a terminal alkyne [29] that will enable initial photocrosslinking of the probe to its targets and latter introduction of biotin using click chemistry. Regarding the linkers, methylenic spacers of 3–5 units, successfully used in the development of other chemical probes [24,30–33], were selected. Taking into account the structure-activity relationship studies that indicate that at least one free hydroxyl group and one allyl group is required for activity [9,10,12], we have studied the influence of different exit vectors at the positions indicated with an arrow (Fig. 1A). Therefore, we designed probes **1**–**4** (Fig. 1B) where the bioactive subunit and the tag are linked by a triazole ring formed through a CuAAC of honokiol-based azides (**5**–**7**, Fig. 1B) and the alkyne of the tag, or viceversa (honokiol-based alkyne **8** and the azide of the tag, Fig. 1B). In addition, we designed the smaller clickable probes **9** and **10** (Fig. 1C), where we have replaced the benzophenone by the less bulky diazirine group as the photocrosslinking moiety, since this latter group offers significant benefits, including decreased steric hindrance and shorter irradiation times. Moreover, in probes **9** and **10**, we have removed the biotin subunit, and introduced instead a terminal alkyne to allow, after incubation with the desired proteome, visualization, enrichment and identification of probe-labeled proteins through a click chemistry reaction with the proper reporter groups (biotin or fluorophore) bearing an azide within their structure.

The preparation of probes **1**–**4** required the synthesis of the honokiol-based fragments **5**–**8** (Fig. 1B). Thus, azide **5** was obtained from 2-bromo-4-chlorophenol, which was alkylated with bromoethane to provide 2-bromo-4-chloro-1-ethoxybenzene (**11**) (Scheme 1). Microwave (MW)-assisted Suzuki coupling of **11** with 4-hydroxyphenylboronic acid led to phenol **12**, whose *O*-allylation followed by Claisen rearrangement of intermediate **13** at low temperature afforded phenol **14**, which was transformed into alcohol **15** by hydroboration-oxidation reaction. The introduction of the allyl chain through the chlorine substituent of **15** required its conversion into the corresponding boronate, which was coupled with allyl bromide to obtain desired intermediate **17**. Finally, transformation of **17** in the mesylate **18** followed by nucleophilic substitution with sodium azide, provided the desired honokiol-based azide **5** (Scheme 1).

Following a similar approach (Scheme 2), Miyaura borylation reaction of chloro derivative **12** yielded boronate **19**, whose Suzuki coupling with allyl bromide, followed by hydroboration-oxidation of the resulting phenol **20**, provided alcohol **21**. *O*-allylation of **21** and Claisen rearrangement of the obtained allyl ether **22**, afforded alcohol **23**, which was transformed into the desired azide **6** through the corresponding mesylate **24** (Scheme 2). Remarkably, allylation of **20**, followed by Claisen rearrangement of the obtained ether **25** provided 2-*O*-ethylhonokiol in 4 steps and 50 % overall yield, whereas the previously described synthetic approach to obtain this derivative was the direct alkylation of honokiol that affords the desired compound in 20 % yield, after purification from the mixture of di- and mono-ethyl derivatives [10,34]. Azide **7** was obtained by etherification of 2-bromo-4-chlorophenol with 3-bromopropan-1-ol, followed by subsequent palladium-catalyzed crosscouplings, *O*-allylation, Claisen rearrangement and activation of the primary alcohol through the corresponding mesylate in analogous manner (Scheme 3).

Finally, synthesis of alkyne **8** was performed as depicted in Scheme 4. Williamson alkylation of 3-bromo-4-hydroxybenzaldehyde with bromoethane, followed by Suzuki coupling of bromoderivative **32** with 4-hydroxyphenylboronic acid yielded biphenyl derivative **33**. *O*-Allylation of phenol **33**, followed by treatment of the resulting aldehyde **34** with ethynylmagnesium bromide, and subsequent reduction of the propargylic alcohol **35** with triethylsilane and trifluoroacetic acid (TFA) provided allyl ether **36**, whose Claisen rearrangement led to the desired alkyne **8**.

Once honokiol-based fragments **5**–**8** were prepared, they were assembled via CuAAC with benzophenone-alkyne or -azide corresponding tags **39** and **40** (Scheme 5), which were obtained by condensation of 4,4′-diaminobenzophenone with biotin using *N*,*N*′-

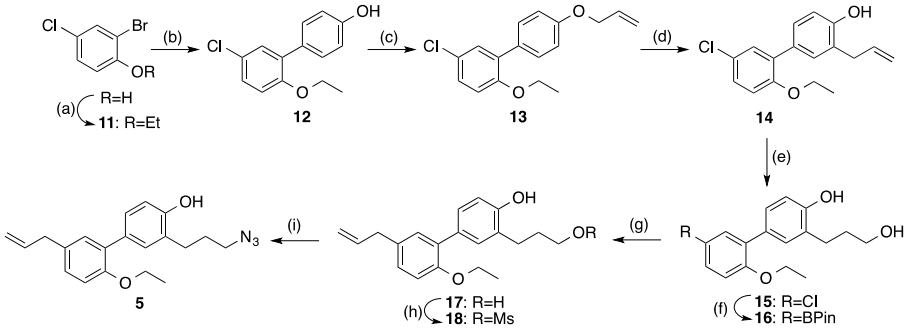


**Scheme 1.** Reagents and conditions: (a) EtBr, $K_2CO_3$, acetone, MW, 140 °C, 96 %; (b) 4-hydroxyphenylboronic acid, $Pd(PPh_3)_4$, $Na_2CO_3$, toluene, EtOH, MW, 110 °C, 92 %; (c) allyl bromide, $K_2CO_3$, acetone, MW, 140 °C, 98 %; (d) $AlMe_3$, $H_2O$, DCM, −20 °C, 90 %; (e) $BH_3$, $H_2O_2$, THF, 0 °C to rt, 84 %; (f) $B_2pin_2$, $Pd_2dba_3$, S–PHOS, KOAc, 1,4-dioxane, MW, 140 °C, 89 %; (g) allyl bromide, $Pd_2dba_3$, $K_2CO_3$, toluene, MW, 150 °C, 60 %; (h) MsCl, pyridine, DCM, −20 °C to rt, 42 %; (i) $NaN_3$, DMF, 60 °C, 70 %.

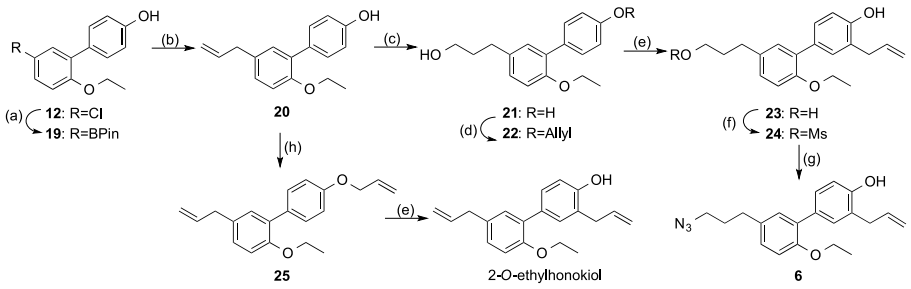


**Scheme 2.** Reagents and conditions: (a) $B_2pin_2$, $Pd_2dba_3$, S–PHOS, KOAc, 1,4-dioxane, MW, 140 °C, 75 %; (b) allyl bromide, $Pd_2dba_3$, $K_2CO_3$, toluene, MW, 150 °C, 75 %; (c) $BH_3$, $H_2O_2$, THF, 0 °C to rt, 53 %; (d) allyl bromide, $K_2CO_3$, acetone, MW, 140 °C, 92 %; (e) $Et_2AlCl$, DCM, −20 °C to 0 °C, 97 %; (f) MsCl, pyridine, DCM, −20 °C to rt, 77 %; (g) $NaN_3$, DMF, 60 °C, 67 %; (h) allyl bromide, $K_2CO_3$, acetone, MW, 140 °C, 92 %.

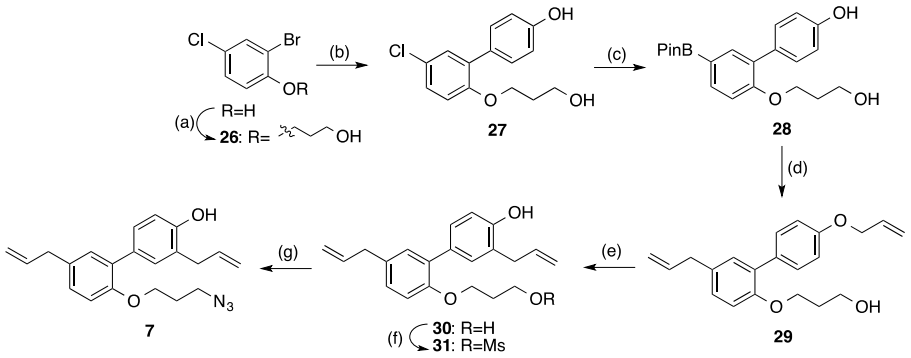


**Scheme 3.** Reagents and conditions: (a) 3-bromopropan-1-ol, $K_2CO_3$, acetone, MW, 140 °C, 85 %; (b) 4-hydroxyphenylboronic acid, $Pd(PPh_3)_4$, $Na_2CO_3$, toluene, EtOH, MW, 110 °C, 82 %; (c) $B_2pin_2$, $Pd_2dba_3$, S–PHOS, KOAc, 1,4-dioxane, MW, 140 °C, 78 %; (d) allyl bromide, $Pd_2dba_3$, $K_2CO_3$, toluene, MW, 150 °C, 47 %; (e) $Et_2AlCl$, DCM, −20 °C to 0 °C, 70 %; (f) MsCl, pyridine, DCM, −20 °C to rt, 53 %; (g) $NaN_3$, DMF, 60 °C, 77 %.

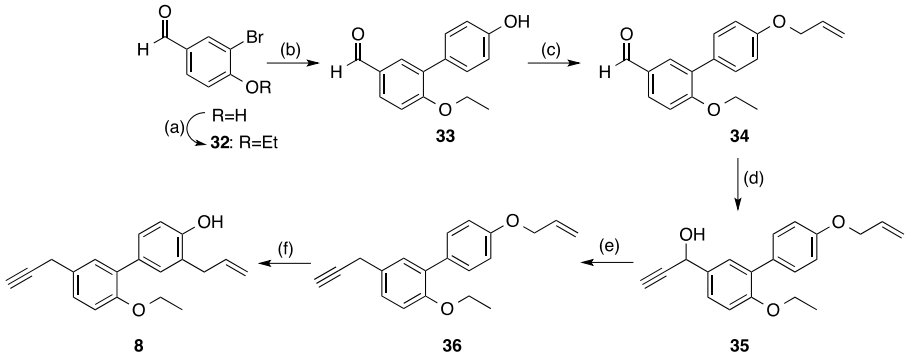


**Scheme 4.** Reagents and conditions: (a) EtBr, $K_2CO_3$, acetone, MW, 140 °C, 89 %; (b) 4-hydroxyphenylboronic acid, $Pd(PPh_3)_4$, $Na_2CO_3$, toluene, EtOH, MW, 110 °C, 68 %; (c) allyl bromide, $K_2CO_3$, acetone, MW, 140 °C, 96 %; (d) ethynylmagnesium bromide, THF, 0 °C to rt, 97 %; (e) $Et_3SiH$, TFA, DCM, 0 °C, 33 %; (f) $Et_2AlCl$, DCM, −20 °C to 0 °C, 51 %.

dicyclohexylcarbodiimide (DCC) and 1-hydroxybenzotriazole (HOBt) in the presence of 4-dimethylaminopyridine (DMAP), and further coupling of the resulting aniline **37** either with 5-hexynoic acid or 6-azidohexanoic acid (**38**).

With respect to probes **9** and **10**, their preparation required the Staudinger reaction of azides **5** and **6** using triphenylphosphine in the presence of water, followed by condensation of the obtained amines **41** and **42** with carboxylic acid **43** (Scheme 6).

### 2.2. Phenotypic screening of honokiol-based probes

In order to identify the targets of honokiol and its derivatives, responsible for their antitumor effects, we first determined whether the synthesized probes kept their biological activity. Among the different malignancies in which honokiol and related compounds have been shown to be antitumorigenic [5], we focused our efforts on the study of their targets in breast and ovarian cancer cell lines since these types of cancer still show dramatically high incidence and mortality rates [35]. Ovarian cancer is the second most prevalent gynaecologic cancer and the most lethal gynaecologic malignancy because of its vague presentation, recurrence, and drug resistance [36]. Regarding breast cancer, among the different subtypes of malignancies based on the expression of estrogen, progesterone, and human epidermal growth factor 2 receptors (ER, PR and HER2, respectively), TNBC -characterized by the absence of the three receptors-deserves special attention. Although TNBC accounts for a low percentage of all breast tumors, it represents a disproportionate number of deaths [37]. For this reason, this group of patients has a very poor prognosis, and therefore the discovery of new targets and drugs for

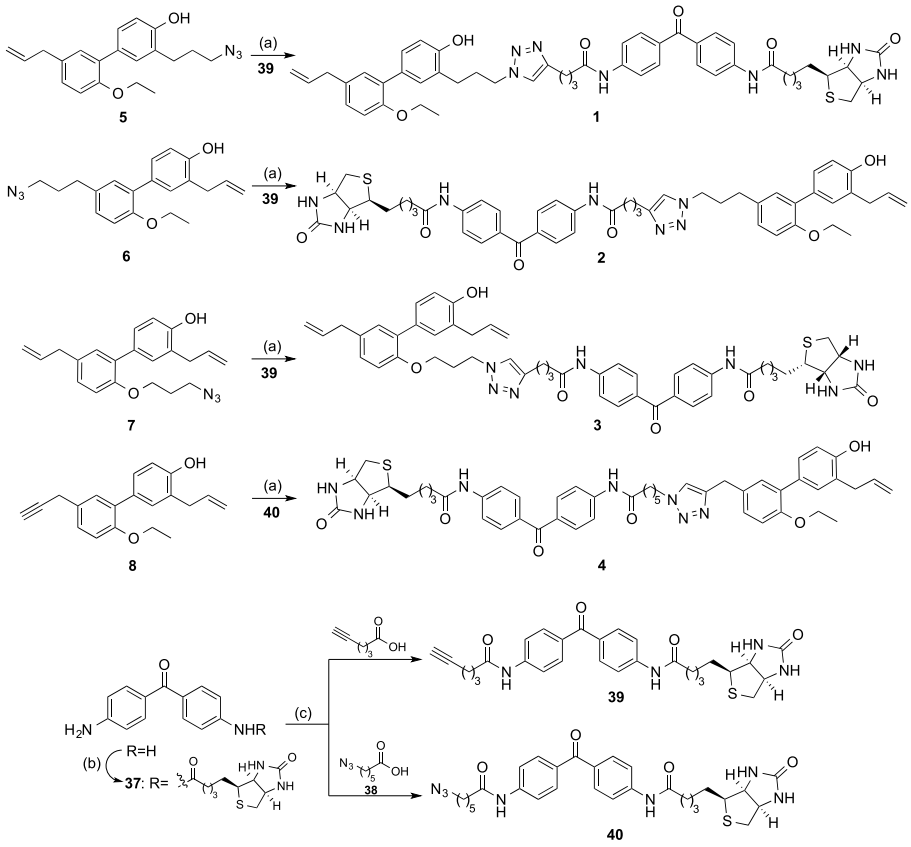

**Scheme 5.** Reagents and conditions: (a) $CuSO_4{\cdot}5H_2O$, sodium ascorbate, DMF, $H_2O$, rt, 25–64 %; (b) biotin, DCC, HOBt, DMAP, DCM, DMF, 77 °C to rt, 97 %; (c) EDC, HOBt, DCM, DMF, rt, 14–36 %.

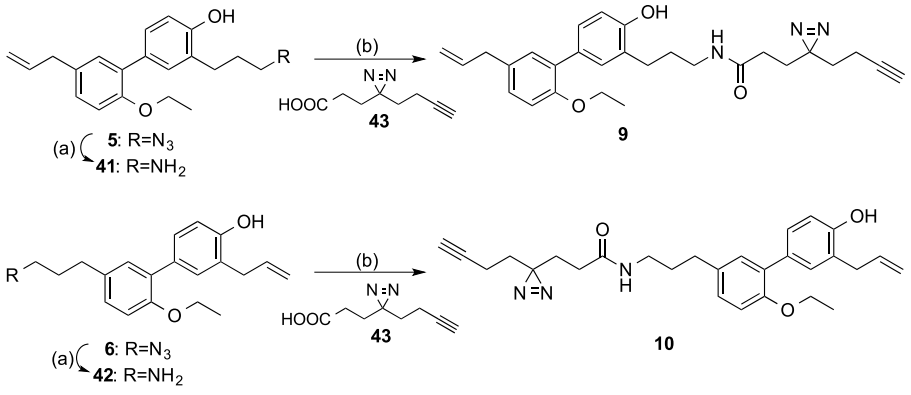

**Scheme 6.** Reagents and conditions: (a) $PPh_3$, THF, $H_2O$, reflux, 49–76 %; (b) EDC, HOBt, DIPEA, DCM, rt, 45–62 %.

the treatment of this disease is an urgent clinical challenge. Hence, the highly aggressive TNBC cell line MDA-MB-231, together with two ovarian cancer cell lines with different invasive potentials, SKOV3 and OVCAR3 (the former one being significantly more invasive than the latter one) [38], were chosen to evaluate the ability of honokiol, 2-*O*-ethylhonokiol and probes **1**–**4**, **9**, and **10** to inhibit cell proliferation (Table 1). The obtained results showed that the introduction of the biotin and benzophenone-containing tags (probes **1**–**4**) significantly reduced their activity when compared with honokiol and 2-*O*-ethylhonokiol. However, the diazirine-containing probes **9** and **10** exhibited good cytotoxic properties, with $IC_{50}$ values similar to honokiol and 2-*O*-ethylhonokiol. These findings are consistent with the bigger size of the tag in compounds **1**–**4** where the presence of the benzophenone moiety and the biotin group may introduce a significant steric hindrance that impairs the binding of the probe to the target protein(s), thus resulting in the inactivity of the compounds. Oppositely, probes **9** and **10** contain a significantly smaller tag, in which diazirine replaces the bulkier benzophenone moiety and biotin has been substituted by a minimalist terminal alkyne. Moreover, both the diazirine and the terminal alkyne have been incorporated in a flexible spacer, feature that introduces a higher degree of conformational freedom in this part of the molecule. This flexibility may facilitate the adequate orientation of the tag towards the outer part of the target protein(s) minimizing potential steric clashes. According to the superior biological activity of probes **9** and **10**, they were selected for further experiments.

**Table 1**
Cell viability studies of honokiol, 2-*O*-ethylhonokiol, and honokiol-based probes **1**–**4**, **9**, and **10** in MDA-MB-231, SKOV3 and OVCAR3 cancer cells.

| Cpd | Cell viability $IC_{50}$ (μM)[a] | | |
|---|---|---|---|
| | MDA-MB-231 | SKOV3 | OVCAR3 |
| Honokiol | 46 ± 2 | 48 ± 1 | 51 ± 2 |
| 2-*O*-Ethylhonokiol | 28 ± 1 | 43 ± 1 | 37 ± 2 |
| **1** | >100 | >100 | >100 |
| **2** | >100 | >100 | >100 |
| **3** | >100 | >100 | >100 |
| **4** | >100 | >100 | >100 |
| **9** | 39 ± 2 | 44 ± 2 | 50 ± 2 |
| **10** | 37 ± 1 | 39 ± 1 | 30 ± 2 |

[a] For those compounds able to reduce cell viability more than 50 % at 50 μM, full dose-response curves were obtained by measuring cell viability 48 h after treatment with compounds at doses between 0 and 200 μM. $IC_{50}$ values were obtained by nonlinear regression (sigmoidal dose-response curve) fitting using GraphPad Prism 10 and they are expressed as the average ± SEM obtained from at least two independent experiments carried out in triplicate.

### 2.3. *In-gel validation of probes 9 and 10*

Before carrying out proteomic experiments, we confirmed that probes **9** and **10** were able to label proteins in a concentration- and UV-dependent manner. In addition, if, as expected, some of the targets are the same as those of honokiol and 2-*O*-ethylhonokiol, their labeling must be competed by an excess of these compounds. In order to assess these aspects, we took advantage of the presence of the terminal alkyne group in probes **9** and **10** to introduce, after cell labeling, a fluorophore suitable for in-gel fluorescence scanning. Briefly, cells were treated with the probes and subjected to UV irradiation to promote covalent binding between the probe and the target proteins. After that, cells were homogenized, the soluble and membrane proteomes separated by centrifugation, and each of these two fractions was reacted with rhodamine-azide (Rh–$N_3$, Fig. 2A) under click chemistry conditions [39]. Finally, proteins were separated by sodium dodecyl-sulfate polyacrylamide gel electrophoresis (SDS-PAGE) and fluorescent bands (corresponding to probe-protein complexes) visualized in a fluorescence scanner. We first evaluated the UV- and concentration-dependent labeling of probes **9** and **10** (0.2–20 μM) in MDA-MB-231 cells. The results shown in Fig. 2B confirm that the labeling is concentration-dependent for both probes, as the intensity of the bands clearly increases with their concentration, ranging from almost no bands for concentrations under 1 μM to intense bands at 10 μM, which seems to reach saturation since no significant increase is noticed at 20 μM. In addition, we observed that the labeling at the highest probe concentration was UV-dependent as in the absence of irradiation only some marginal non-specific fluorescence was detected (see UV negative lanes in Fig. 2B).

Then, we performed competition experiments in the presence of an excess of honokiol and 2-*O*-ethylhonokiol (H and EH, respectively, in Fig. 3) to ensure that at least some of the labeled proteins were targets of these compounds. Remarkably, some of the bands disappeared in the presence of an excess of honokiol and 2-*O*-ethylhonokiol both in membrane and soluble fractions (see some representative examples marked with an orange arrowhead in Fig. 3). This result indicates that probes **9** and **10** are indeed labeling some of the targets of the honokiol family of compounds in MDA-MB-231 cells.

In order to establish the generality of the approach, we extended the use of the probes to ovarian cancer cell lines. Taken into account the

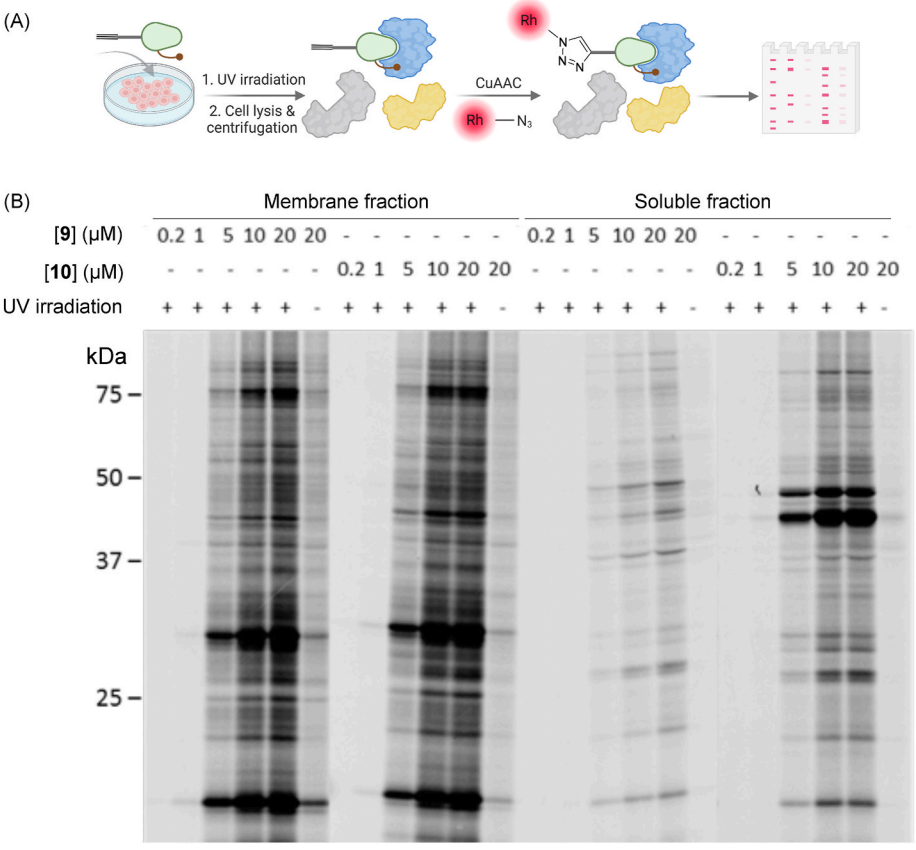


**Fig. 2.** (A) Schematic representation of the proteomic platform for the visualization of probe-labeled proteins by in-gel fluorescence scanning after click chemistry with rhodamine-azide ($RhN_3$). (B) Concentration- and UV-dependent labeling of MDA-MB-231 breast cancer cells by probes **9** and **10**. Irradiation is carried out at 365 nm for 10 min. Fluorescence is shown in grey scale. All lanes contained 20 μg of total protein and equal loading was confirmed by Coomassie brilliant blue staining (see Figure S1 in the Supplementary data).

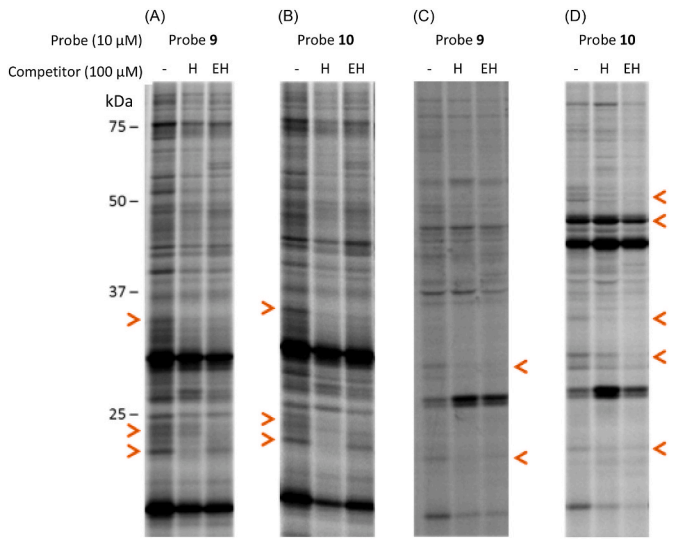


**Fig. 3.** Competition of probes **9** (A, C) and **10** (B, D) at 10 μM by honokiol (H) or 2-*O*-ethylhonokiol (EH) at 100 μM in membrane (A, B) and soluble (C, D) proteomes, respectively, in MDA-MB-231 breast cancer cells. Fluorescence is shown in grey scale. Arrowheads show some representative competed proteins. All lanes contained 20 μg of total protein and equal loading was confirmed by Coomassie brilliant blue staining (see Figure S2 in the Supplementary data).

superior ability of probe **10** to label proteins compared to probe **9**, especially in the soluble proteome (Fig. 3) (which is in agreement to the superior cytotoxic capacity of **10** compared to **9**, see Table 1), this probe was selected to establish the labeling pattern in SKOV3 and OVCAR3 cells (Fig. 4). The obtained results indicate that both honokiol and 2-*O*-ethylhonokiol target specific proteins in these cell lines. These targets are those bands present in the probe-treated proteomes and which disappear in the presence of an excess of honokiol and/or 2-*O*-ethylhonokiol. Some representative examples are marked with an orange arrowhead (bands present in both cell lines) and with a green arrowhead (bands present predominantly in one of the two cell lines) (Fig. 4).

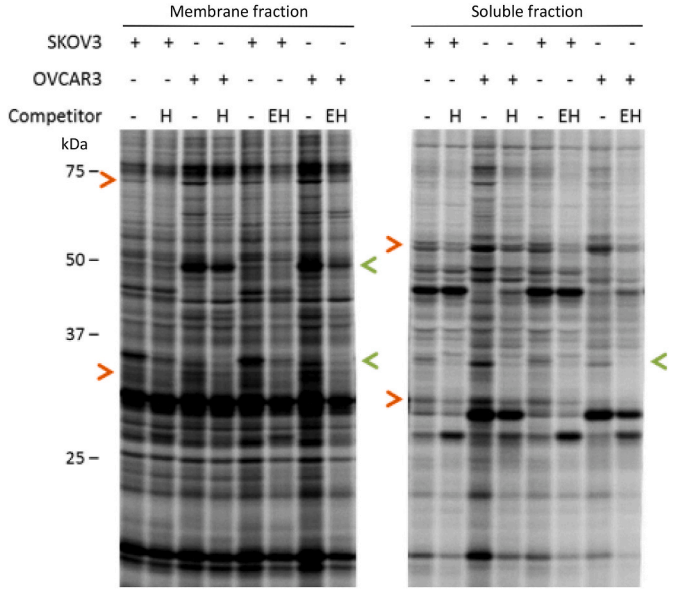


**Fig. 4.** Labeling pattern of probe **10** in the ovarian cancer cell lines SKOV3 and OVCAR3. Competition of probe **10** at 10 μM by honokiol (H) or 2-*O*-ethylhonokiol (EH) at 100 μM in membrane (left panel) and soluble (right panel) proteomes. Fluorescence is shown in grey scale. Arrowheads show some representative bands. All lanes contained 20 μg of total protein and equal loading was confirmed by Coomassie brilliant blue staining (see Figure S3 in the Supplementary data).

In summary, the in situ profiling in MDA-MB-231 (Figs. 2 and 3) and ovarian (Fig. 4) cancer cell lines confirms the suitability of probes **9** and **10** for identifying the targets of honokiol and 2-*O*-ethylhonokiol in these systems. Collectively, these results underscore the notion that the described probes can selectively interact with protein targets in a context-specific manner, as shown by the differences in labeling obtained between the two ovarian cancer cell lines (Fig. 4) or between ovarian and breast cancer cell lines (Figs. 3 and 4), thereby warranting further in-depth analysis to identify differential protein targets through quantitative MS-based chemical proteomics. Considering that the best results have been obtained for probe **10** in MDA-MB-231 cells, these are the conditions selected for carrying out the chemical proteomic experiments.

### 2.4. *Proteomic profiling of probe 10*

Proteins targeted by probe **10** were enriched and identified using stable isotope labeling by amino acids in cell culture (SILAC) quantitative MS. In SILAC experiments, two groups of cells are grown in parallel using the same culture media but with at least one essential amino acid isotopically labeled in one of the groups (termed heavy), while the same amino acid is the light version in the other group. Since cells are not able to synthesize essential amino acids, they are forced to use only the externally supplied one, eventually incorporating 100 % of the given "light'' or "heavy'' amino acid in all the proteins. Finally, after lysing the "heavy" and "light" cells, they can be combined and the mixture can be treated as a single sample in all subsequent steps. Hence, once the final sample has been trypsinized, SILAC peptide pairs have the same retention time, but different mass, thus enabling the measurement of the ratio between both peptides, referred to as SILAC ratio, providing an accurate method for quantification of the labeled proteins [40].

MDA-MB-231 cells were cultured in the presence of either the heavy version of Lys ($^{13}C_6$, $^{15}N$) and Arg ($^{13}C_6$, $^{15}N_4$) or their light versions ($^{12}C_6$, $^{14}N$-Lys; $^{12}C_6$, $^{14}N_4$-Arg). for at least six cell doublings to ensure complete incorporation of the light or heavy version of the amino acids in all the proteins. Then, "heavy" cells were incubated with 10 μM of probe **10**, and "light" cells with 10 μM of probe **10** plus 100 μM of honokiol. Both samples were UV-irradiated, homogenized and mixed in a 1:1 ratio (Fig. 5A). After that, the sample was coupled to a biotin-azide reporter tag (biotin-$N_3$, Fig. 5B) under click chemistry conditions, and probe-protein complexes were captured by incubation with streptavidin beads. After digestion with trypsin, the obtained peptides were separated by LC and identified by MS according to the experimental protocol previously optimized [39]. The resulting SILAC ratios were normalized in a 1–20 scale, where a ratio of 1 indicates no difference between the light and heavy labeled samples, and therefore no competition by honokiol, and 20 is the maximal difference. Fig. 5C shows the heavy:light SILAC ratio plot for all the identified proteins using probe **10**. Proteins that exhibited SILAC ratios ≥3 were designated as preferred targets of honokiol (Fig. 5C, insert). Therefore, the use of probe **10** enabled the identification of 42 proteins that were significantly competed by honokiol (Table 2).

Term enrichment analysis from the gene-disease association database DisGeNET [57] (Fig. 6A) revealed a preferential implication of the identified proteins in cancer (26 out of 42 proteins) of different origins but with special overrepresentation of breast (12 out of the 26 proteins), liver (5 proteins) and renal (3 proteins) carcinomas as well as malignant neoplasm of mouth and squamous cell carcinoma of esophagus (5 proteins) together with other proteins involved in tumor metastasis or invasiveness processes regardless the tissue of origin (full set of data is shown in Supplementary Table 1, Supplementary data). This is highly consistent with the described antitumor properties of honokiol [58,59]. Notably, the antitumor properties of honokiol in breast cancer have been mainly related to apoptosis induction and cell cycle arrest [8,60], while

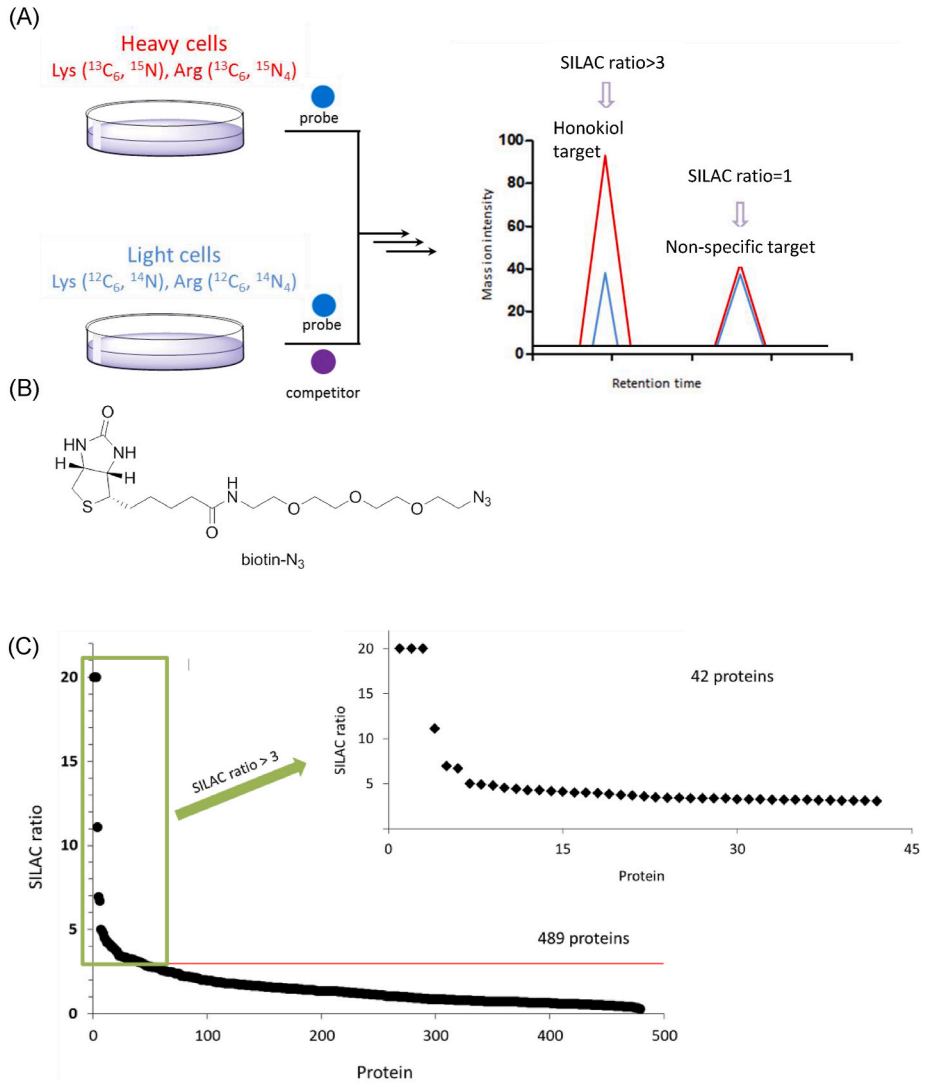


**Fig. 5.** (A) Scheme of the proteomic platform for the preparation of SILAC samples. (B) Structure of the biotin-azide reporter tag. (C) SILAC ratio plots for total proteins and for proteins with a SILAC ratio≥3, identified comparing cells treated with probe **10** at 10 μM versus probe **10** at 10 μM plus honokiol at 100 μM.

the effect in renal carcinoma has been linked to cell migration and metastasis inhibition [61–63]. Similarly, the antitumor properties in liver carcinoma has been mechanistically linked to the inhibition of migration and induction of apoptosis [64–66]. Finally, most cancers derived from the mucosal epithelium in the oral cavity, pharynx and larynx fall into the category known collectively as head and neck squamous cell carcinoma (HNSCC), and more than 90 % of mouth cancers are squamous cell carcinomas [67]. Honokiol has been linked to anticancer effects in HNSCC [13,68,69] mainly through induction of apoptosis and cell cycle arrest. Collectively, these results are in accordance with the enrichment in proteins related to apoptosis and metabolic processes revealed by gene ontology (GO) and protein annotation through evolutionary relationship (PANTHER) analysis [70], which showed that the majority of the identified proteins are implicated in metabolic processes (N = 30, 71 %) or in the regulation of apoptosis (N = 13, 31 %) (Fig. 6B), two key hallmarks of cancer [71–73]. Remarkably, half of the identified proteins exhibit cancer dependencies as described in the cancer dependency map (DepMap project). Specifically, a significant number (N = 10, 24 %) are defined as common essential to indicate their general requirement of the growth of most cancer cells, and 26 % are defined as strongly selective in the cancer dependency map (Fig. 6C), further supporting the significance of the data in relation to the antitumor potential of honokiol. Enriched proteins belong to different functional and structural classes, enzymes being more than half of the identified proteins. With respect to their cellular location, most of the identified proteins are located in the mitochondria (N = 18, 43 %) or in the cell junction (N = 10, 24 %) being the rest in the cytosol (N = 14, Fig. 6D). This is highly consistent with the role of the proteins in tumor processes, migration and energy control. Mitochondria can influence all processes linked to oncogenesis, starting from malignant transformation to metastatic dissemination and are pivotal regulators in the processes of programmed cell death, including apoptosis [74–77]. Furthermore, honokiol has been reported to localize in mitochondria [78] and to mediate antiproliferative effects through mitochondria-mediated death signaling [79–81]. The second main group, which comprises proteins located primarily in the cell junction, represents cytoskeletal-associated proteins such as lyric protein (also known as metadherin or AEG-1), vimentin, ezrin or moesin, which have been related to epithelial-mesenchymal transition (EMT), migration and metastasis featured by cancer cells [82–84]. Interestingly, honokiol has been previously linked to the reversal of EMT and the induction of a decrease in the levels of vimentin [53,85,86].

Further analysis using the Database for Annotation, Visualization and Integrated Discovery (DAVID) [87,88] revealed a strong enrichment in post-translationally modified proteins, being acetylation present in 37 out of the 42 identified proteins (88 %) and phosphorylation present in

**Table 2**
Proteins with SILAC ratio≥3.

| SILAC ratio | Uniprot Access. Number | Protein | Biological Process[a] | DAVID Disgenet[b] | Cancer dependency Map Status[c] | Known cpds[d] | Previously related to honokiol |
|---|---|---|---|---|---|---|---|
| 20.0 | Q86UE4 | Lyric Metadherin | Regulation of programmed cell death | Breast carcinoma | NA | No | No |
| 20.0 | P52209 | PGD 6-phosphogluconate dehydrogenase, decarboxylating | Metabolic process | Liver carcinoma | Common essential | Yes | No |
| 20.0 | P53396 | ACLY ATP-citrate synthase | Metabolic process | Liver carcinoma | Common essential | Yes | No |
| 11.1 | P07384 | CAPN1 Calpain-1 catalytic subunit | Metabolic process | Other, tumorigenesis and metastasis [41] | NA | Yes | Partially [42] |
| 7.0 | Q9BWD1 | ACAT2 Acetyl-CoA acetyltransferase, cytosolic | Metabolic process | Other, ovarian cancer [43], esophageal squamous cell carcinoma [44] | Strongly selective | No | No |
| 6.7 | P43490 | NAMPT Nicotinamide phosphoribosyl-transferase | Metabolic process | Malignant neoplasm of mouth | Strongly selective | Yes | Partially [45] |
| 5.0 | P29401 | TKT Transketolase | Metabolic process | Mammary carcinoma | Strongly selective | Yes | No |
| 4.9 | P07339 | CTSD Cathepsin D | Metabolic process, Regulation of programmed cell death | Liver carcinoma, renal cell carcinoma | NA | Yes | Partially [46] |
| 4.8 | P40926 | MDH2 Malate dehydrogenase, mitochondrial | Metabolic process | Mammary carcinoma | Strongly selective | No | No |
| 4.5 | P00367 | GLUD1 Glutamate dehydrogenase 1, mitochondrial | Metabolic process | Other | NA | No | No |
| 4.4 | P04181 | OAT Ornithine aminotransferase, mitochondrial | Metabolic process | Liver cirrhosis | NA | Yes | No |
| 4.3 | P36776 | LONP1 Lon protease homolog, mitochondrial | Metabolic process | Other, cancer [47] | Common essential | Yes | No |
| 4.2 | P46821 | MAP1B Microtubule-associated protein 1B | Regulation of cellular location | Other | NA | No | No |
| 4.1 | P07195 | LDHB l-lactate dehydrogenase B chain | Metabolic process | Breast carcinoma, renal cell carcinoma | Strongly selective | Yes | Partially [48] |
| 4.1 | P39687 | ANP32A Acidic leucine-rich nuclear phosphoprotein 32 family | Regulation of programmed cell death | Colorrectal carcinoma, adenocarcinoma of lung | NA | No | No |
| 4.0 | P24752 | ACAT1 Acetyl-CoA acetyltransferase, mitochondrial | Metabolic process | Liver cirrhosis | Strongly selective | Yes | No |
| 4.0 | P62937 | PPIA Peptidyl-prolyl *cis*-trans isomerase A | Metabolic process, Regulation of programmed cell death | Malignant neoplasm of the mouth, squamous cell carcinoma | NA | Yes | Partially [49] |
| 3.9 | P11498 | PC Pyruvate carboxylase, mitochondrial | Metabolic process | Liver cirrhosis, metastasis [50] | Strongly selective AND common essential | No | No |
| 3.8 | P10809 | HSPD1 60 kDa heat shock protein, mitochondrial | Metabolic process, Regulation of programmed cell death | Renal cell carcinoma | Common essential | No | Partially [51] |
| 3.7 | P49327 | FASN Fatty acid synthase | Metabolic process | Breast carcinoma | Strongly selective | Yes | No |
| 3.7 | P14618 | PKM Pyruvate kinase isozymes M1/M2 | Metabolic process | Mammary carcinoma, liver carcinoma | Common essential | Yes | No |
| 3.6 | P26038 | MSN Moesin | Membrane to membrane docking | Liver cirrhosis | NA | No | No |
| 3.5 | P23526 | AHCY Adenosylhomo-cysteinase | Metabolic process | Other | NA | Yes | No |
| 3.4 | P07900 | HSP90AA1 Heat shock protein HSP 90-alpha | Metabolic process, Regulation of programmed cell death | Breast carcinoma | NA | Yes | Partially [52] |
| 3.4 | Q01105 | SET Protein SET | Metabolic process, Regulation of programmed cell death | Neoplasm invasiveness | NA | No | No |
| 3.4 | Q9NY33 | DPP3 Dipeptidyl peptidase 3 | Metabolic process | Other | NA | No | No |

(*continued on next page*)

**Table 2** (*continued*)

| SILAC ratio | Uniprot Access. Number | Protein | Biological Process[a] | DAVID Disgenet[b] | Cancer dependency Map Status[c] | Known cpds[d] | Previously related to honokiol |
|---|---|---|---|---|---|---|---|
| 3.4 | P31948 | STIP1 Stress-induced-phosphoprotein 1 | Cellular response to interleukin-7 | Breast cancer | NA | No | No |
| 3.4 | P06733 | ENO1 Alpha-enolase | Metabolic process, Regulation of programmed cell death | Breast carcinoma | NA | Yes | No |
| 3.3 | P06737 | PYGL Glycogen phosphorylase, liver form | Metabolic process | Liver carcinoma | NA | Yes | No |
| 3.3 | P08670 | VIM Vimentin | Cell differentiation | Breast carcinoma | NA | No | Partially [53] |
| 3.2 | P47897 | QARS Glutamine–tRNA ligase | Metabolic process, Regulation of programmed cell death | Other, glioblastoma [54] | Common essential | No | No |
| 3.2 | P60174 | TPI1 Triosephosphate isomerase | Metabolic process | Malignant neoplasm of the mouth, squamous cell carcinoma of esophagus, adenocarcinoma of lung | Common essential | No | No |
| 3.2 | Q86VP6 | CAND1 Cullin-associated NEDD8-dissociated protein 1 | Metabolic process | Other | NA | No | No |
| 3.2 | P07737 | PFN1 Profilin-1 | Development | Squamous cell carcinoma of esophagus | Common essential | No | No |
| 3.2 | P15311 | EZR Ezrin | Membrane to membrane docking | Mammary carcinoma | Strongly selective | No | No |
| 3.2 | O00299 | CLIC1 Chloride intracellular channel protein 1 | Cell differentiation | Breast carcinoma, squamous cell carcinoma of esophagus | NA | No | No |
| 3.2 | P22314 | UBA1 Ubiquitin-like modifier-activating enzyme 1 | Metabolic process | Squamous cell carcinoma | Common essential | Yes | No |
| 3.2 | P22392 | NME2 Nucleoside diphosphate kinase B | Metabolic process, Regulation of programmed cell death | Colorectal neoplasm | Common essential | No | No |
| 3.1 | O43707 | ACTN4 Alpha-actinin-4 | Regulation of programmed cell death | Mammary carcinoma | NA | No | No |
| 3.1 | P08238 | HSP90AB1 Heat shock protein HSP 90-beta | Metabolic process, Regulation of programmed cell death | Other, cancer [55] | Strongly selective | Yes | Partially [52] |
| 3.1 | P62258 | YWHAE 14-3-3 protein epsilon | Cellular response to heat | Neoplasm metastasis | NA | No | No |
| 3.0 | Q96TA1 | FAM129B Niban-like protein 1 | Regulation of programmed cell death | Melanoma [56] | Strongly selective | No | No |

[a] Biological processes according to the gene onthology (GO) annotations.
[b] Enriched functional associations with diseases according to related gene groups from the Database for Annotation, Visualization and Integrated Discovery (DAVID) and the gene-disease association database DisGeNET except when a specific reference is given.
[c] Cancer dependencies as described in the cancer dependency map (DepMap project) with NA meaning that no significant cancer dependency has been found.
[d] Known bioactive compounds acting in the indicated protein as described in the cancer dependency map database.

35 out of 42 (83 %) (Fig. 6E). These modifications are highly abundant in mitochondrial proteins and have been linked to cancer [89–93], and, remarkably, honokiol has been reported to decrease the levels of acetylated mitochondrial proteins [94].

In addition, according to the cancer dependency map, more than half of the identified hits (N = 23) lack known bioactive compounds, so the compounds described here could be initial hits to ease the development of potent, selective, and specific chemical probes for these proteins.

Some of the identified targets, such as calpain-1, nicotinamide phosphoribosyltransferase, cathepsin D, lactate dehydrogenase, peptidyl-prolyl *cis*-trans isomerase A, heat shock proteins HSP60 and 90, and vimentin have been previously related with honokiol [42,45,46,48,49,51–53], thus supporting the significance of these findings. However, the studies reported so far have not generally addressed the direct interaction between honokiol and these proteins, so we selected some of the identified targets for validation.

### 2.5. Validation of selected proteins

To select the candidates for validation we focused our attention in the top candidates, i.e., those proteins with SILAC ratio>10, as well as in those proteins without a relevant presence in the CRAPome database (www.crapome.org), which include those proteins consistently appearing as background contaminants under control conditions in pull-down experiments [95]. In this way, we selected lyric, 6-phosphogluconate dehydrogenase decarboxylating (PGD), and calpain-1 (CAPN-1) proteins for validation. In addition, we have also considered dipeptidyl peptidase 3 (DPP3), as an example of a protein with a moderate SILAC ratio (3.4-fold) but with a <5 % appearance in the crapome database, to support the suitability of all identified proteins as bona fide interactors.

The direct interaction between honokiol and the selected proteins has been evaluated by cellular thermal shift assay (CETSA), which is based on the fact that thermal stability of proteins changes upon ligand binding, and that this change can be assessed by a thermal shift in the melting curve of the protein in the presence of the ligand [96]. Accordingly, we incubated MDA-MB-231 cells with honokiol (10 μM) and studied the thermal stability of lyric protein, DPP3, PGD, and CAPN-1. As shown in Fig. 7, honokiol increased the thermal stability of all four proteins ranging from 1 °C for lyric protein to 4.3 °C for CAPN-1. This result strongly suggests that the proteins identified in this study may represent genuine target proteins for honokiol, at least in breast cancer cell lines. Interestingly, PGD, lyric protein and CAPN-1 regulate

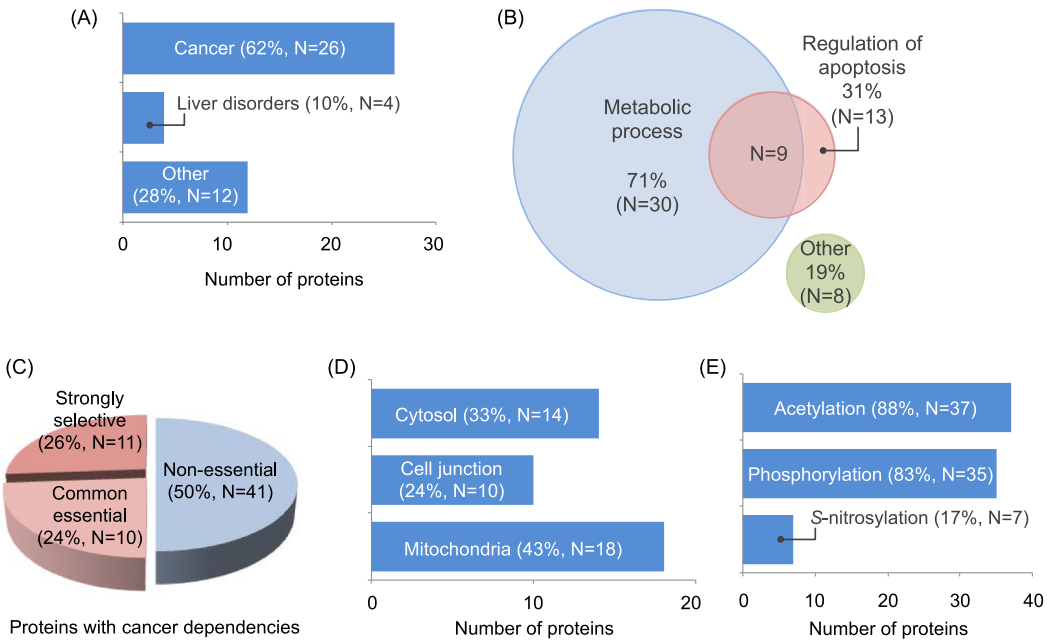


**Fig. 6.** Analysis of honokiol-interacting proteins. (A) Functional associations with diseases according to the Database for Annotation, Visualization and Integrated Discovery (DAVID) and the gene-disease association database DisGeNET term enrichment analysis. (B) Biological process enrichment revealed by gene onthology (GO) and protein annotation through evolutionary relationship (PANTHER) analysis. (C) Proteins defined as strongly selective in the cancer dependency map, reflecting a restricted dependency relationship with specific cancer cell lines, and as common essential to indicate their general requirement for proliferation of most cancer cell lines regardless of their tissue origin. (D) Cellular component enrichment revealed by GO and PANTHER analysis. (E) Post-translational modification enrichment according to DAVID.

mechanisms associated to the viability of cancer cells such as apoptosis, cell proliferation or cell growth. For example, lyric protein triggers diverse oncogenic signaling cascades including PI3K/AKT/mTOR, MAPK, Wnt and NF-κB [97], pathways that have been previously related to the antitumor action of honokiol [5]. PGD has been related to tumor growth and its inhibitors have been described to reduce cancer cell proliferation and tumor growth in nude mice xenografts [98], and CAPN-1 is an essential protease involved in processes like apoptosis, proliferation, and cell migration, and whose deregulation has been linked to cancer [41].

## 3. Conclusions

Collectively, the results reported herein provide, for the first time, direct insights into the mechanism of action of honokiol and its derivatives, aiding to the identification of new targets for addressing currently unmet medical needs. In addition, the synthetic routes developed in this work facilitate accessibility to a series of structurally diverse derivatives of honokiol to carry out systematic structure-activity relationship studies to fully uncover its biological potential.

## 4. Experimental part

### 4.1. Chemistry

Unless stated otherwise, starting materials, reagents and solvents were purchased as high-grade commercial products from Abcr, Acros, Scharlab, Sigma-Aldrich, or Thermo Fisher Scientific, and were used without further purification. All non-aqueous reactions were performed under an argon atmosphere in oven-dried glassware. Tetrahydrofuran (THF), diethyl ether, and dichloromethane (DCM) were dried using a Pure SolvTM Micro 100 L solvent purification system. Acetone was dried under $K_2CO_3$. Pyridine was dried over KOH and distilled before use. Reactions under MW irradiation were performed in a Biotage Initiator 2.5 reactor. Reactions were monitored by analytical thin-layer chromatography (TLC) on silica gel plates supplied by Merck (Kieselgel 60 F-254) with detection by UV light (254 nm) or 10 % phosphomolybdic acid solution in EtOH. Flash chromatography was performed on a Varian 971-FP flash purification system using silica gel cartridges (Varian, particle size 50 μm) or on glass columns. Melting points (mp, uncorrected) were determined on a Stuart Scientific electrothermal apparatus. Infrared (IR) spectra were measured on a Bruker Tensor 27 instrument equipped with a Specac ATR accessory of 5200-650 $cm^{-1}$ transmission range; frequencies ($\nu$) are expressed in $cm^{-1}$. Nuclear Magnetic Resonance (NMR) spectra were recorded on a Bruker Avance III 700 MHz ($^1$H, 700 MHz; $^{13}$C, 175 MHz), Bruker Avance 500 MHz ($^1$H, 500 MHz; $^{13}$C, 125 MHz), or Bruker DPX 300 MHz ($^1$H, 300 MHz; $^{13}$C, 75 MHz) instruments at the Universidad Complutense de Madrid (UCM) NMR core facilities. Chemical shifts (δ) are expressed in parts per million relative to internal tetramethylsilane; coupling constants (*J*) are in hertz (Hz). The following abbreviations are used to describe peak patterns when appropriate: s (singlet), d (doublet), t (triplet), q (quartet), qt (quintet), m (multiplet), br (broad), app (apparent). 2D NMR experiments -homonuclear correlation spectroscopy (H,H–COSY), heteronuclear multiple quantum correlation (HMQC) and heteronuclear multiple bond correlation (HMBC)- of representative compounds were carried out to assign protons and carbons of the new structures. High resolution mass spectrometry (HRMS) was carried out on a Bruker FTMS APEX-Q-IV spectrometer in electrospray ionization (ESI) mode or on a Bruker MALDI-TOF/TOF ULTRAFLEX spectrometer at the UCM's mass spectrometry core facility. High performance liquid chromatography coupled to mass spectrometry (HPLC-MS) analysis was performed using an Agilent 1200LC-MSD VL instrument. LC separation was achieved with a Zorbax Eclipse XDB-C18 column (5 μm, 4.6 mm × 150 mm) or a Zorbax SB-C3 column (5 μm, 2.1 mm × 50 mm), both together with a guard column (5 μm, 4.6 mm × 12.5 mm). The gradient mobile phases consisted of A (95:5 water/acetonitrile) and B (5:95 water/acetonitrile) with 0.1 % ammonium hydroxide and 0.1 % formic acid as the solvent modifiers. MS analysis was performed with an ESI source. The capillary voltage was set to 3.0 kV and the fragmentor voltage was set at 72 eV.

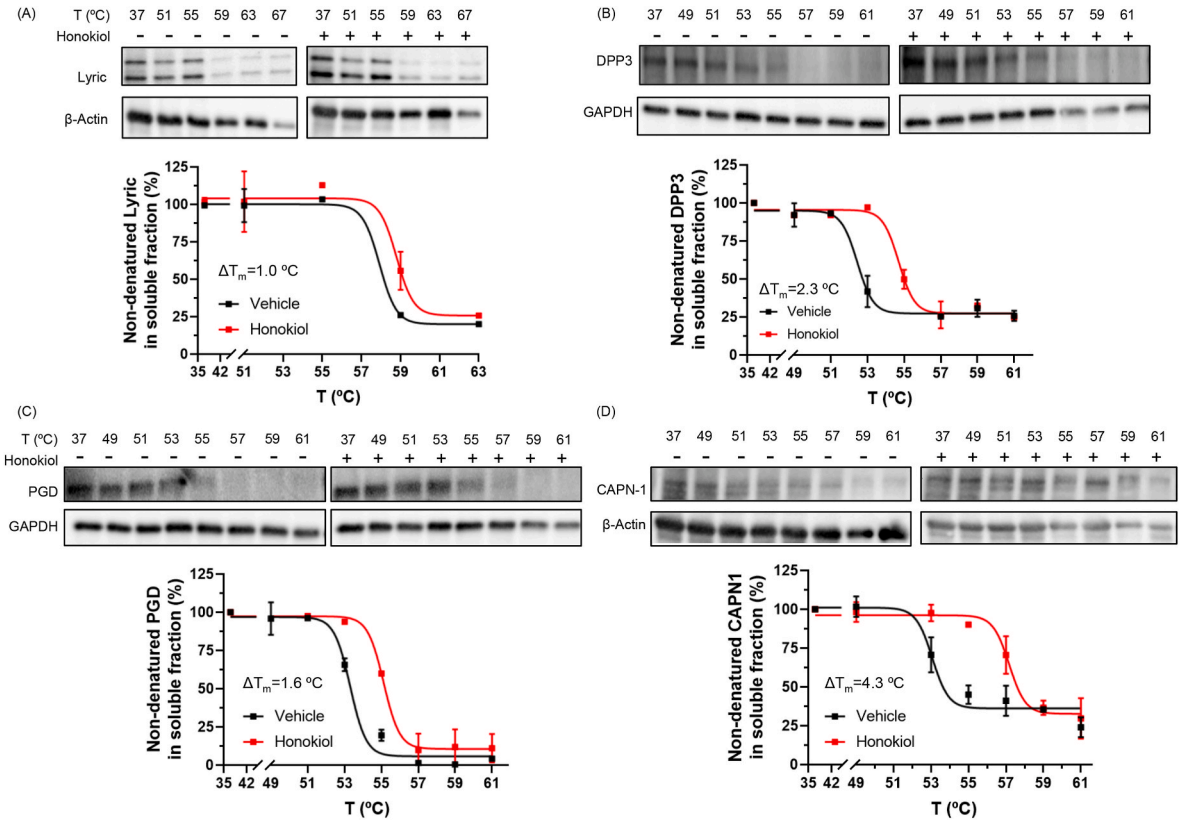


**Fig. 7.** CETSA assays for (A) lyric, (B) DPP3, (C) PGD and (D) CAPN-1 proteins. Representative immunoblotting of the soluble fractions of MDA-MB-231 cells treated with 10 μM of honokiol or vehicle as indicated in the figure and heat-shocked at the indicated temperature, and thermal denaturation curves of the corresponding protein in the presence of vehicle (black) or honokiol (red) as indicated in the figure. Curves are generated and fitted using a four-parameter nonlinear regression curve fit in GraphPad Prism. Band intensities were normalized with respect to the loading controls and percentage of non-denatured protein is expressed respect to the value obtained at 37 °C. Symbols and associated error bars (when not enclosed by the symbol) represent mean ± SD from at least two independent experiments carried out in duplicate.

The drying gas temperature was 350 °C, the drying gas flow was 10 L/min, and the nebulizer pressure was 20 psi. Spectra were acquired in positive or negative ionization mode from 100 to 1200 *m/z* and in UV-mode at four different wavelengths (210, 230, 254, and 280 nm). Optical rotation [α] was measured on an Anton Paar MCP 100 modular circular polarimeter using a sodium lamp (λ = 589 nm) with a 1 dm path length; concentrations (c) are given as g/100 mL. Satisfactory HPLC-MS chromatograms were obtained for all tested compounds, which confirmed a purity of at least 95 %.

The following compounds were synthesized as previously described and their spectroscopic data correspond with those reported: 6-azidohexanoic acid (**38**) [99], 3-[3-(but-3-yn-1-yl)-3*H*-diazirin-3-yl]propanoic acid (**43**) [39], and *N*-(3-azidopropyl) tetramethylrhodamine-5-(and-6)-carboxamide (rhodamine-azide, Rh–$N_3$) [100].

### 4.1.1. General procedure 1

*Williamson alkylation of phenols.* To a solution of the corresponding phenol (1 equiv) in dry acetone (7.5 mL/mmol) under an argon atmosphere, $K_2CO_3$ (1.2 equiv) was added at rt and the mixture was stirred for 10 min. The corresponding bromoalkane (1.2 equiv) was then added and the reaction was heated at 140 °C for 20 min under MW irradiation. Once cooled to rt, water was added and the mixture was extracted with EtOAc (2x), washed with brine, dried ($Na_2SO_4$), filtered, and evaporated under reduced pressure. The crude was purified by chromatography using the appropriate eluent to afford the corresponding aryl alkyl ethers **11**, **13**, **22**, **25**, **26**, **32**, and **34**.

*2-Bromo-4-chloro-1-ethoxybenzene **(11)**.* Obtained from 2-bromo-4-chlorophenol (2.00 g, 9.6 mmol) and bromoethane (0.9 mL, 12 mmol) in 96 % yield (2.20 g). Chromatography: hexane.

*4'-(Allyloxy)-5-chloro-2-ethoxybiphenyl **(13)**.* Obtained from phenol **12** (157 mg, 0.63 mmol) and allyl bromide (60 μL, 0.70 mmol) in 98 % yield (178 mg). It was used in the next step without further purification.

*3-[4'-(Allyloxy)-6-ethoxybiphenyl-*3-yl*]propan-1-ol **(22)**.* Obtained from phenol **21** (220 mg, 0.81 mmol) and allyl bromide (84 μL, 0.97 mmol) in 92 % yield (235 mg). This compound was used in the next step without further purification.

*5-Allyl-4'-(allyloxy)-2-ethoxybiphenyl **(25)**.* Obtained from phenol **20** (30 mg, 0.12 mmol) and allyl bromide (13 μL, 0.14 mmol) in 92 % yield (32 mg). It was used in the next step without further purification.

*3-(2-Bromo-4-chlorophenoxy)propan-1-ol **(26)**.* Obtained from 2-bromo-4-chlorophenol (2.00 g, 9.6 mmol) and 3-bromopropan-1-ol (1.0 mL, 12 mmol) in 85 % yield (2.20 g). Chromatography: hexane to hexane/EtOAc, 7:3.

*3-Bromo-4-ethoxybenzaldehyde **(32)**.* Obtained from 3-bromo-4-hydroxybenzaldehyde (600 mg, 3.0 mmol) and bromoethane (0.3 mL, 3.6 mmol) in 89 % yield (612 mg). Chromatography: hexane to hexane/EtOAc, 9:1.

*4'-(Allyloxy)-6-ethoxy-1,1'-biphenyl-3-carbaldehyde **(34)**.* Obtained from phenol **33** (134 mg, 0.55 mmol) and allyl bromide (72 μL, 0.83 mmol) in 96 % yield (149 mg). Chromatography: hexane to hexane/EtOAc, 8:2.

### 4.1.2. General procedure 2

*Suzuki coupling of bromoderivatives and 4-hydroxyphenylboronic acid.* To a solution of the corresponding bromoderivative (1 equiv) and 4-hydroxyphenylboronic acid (1.5 equiv) in a mixture of toluene/EtOH 1:1 (12 mL/mmol) a solution of 0.5 M $Na_2CO_3$ (aq, 3 equiv) was added

and the mixture was degassed with argon. Then, $Pd(PPh_3)_4$ (0.06 equiv) was added and the reaction mixture was heated at 110 °C for 15 min under MW irradiation. The organic phase was separated, and the aqueous layer was extracted with EtOAc (2x). The combined organic extracts were washed with brine, dried ($Na_2SO_4$), filtered, and evaporated under reduced pressure. The crude was purified by chromatography using the appropriate eluent to afford the corresponding biphenyl derivatives **12**, **27**, and **33**.

*5′-Chloro-2′-ethoxybiphenyl-4-ol **(12)***. Obtained from bromoderivative **11** (100 mg, 0.42 mmol) and 4-hydroxyphenylboronic acid (88 mg, 0.64 mmol) in 92 % yield (96 mg). Chromatography: hexane to hexane/EtOAc, 9:1.

*5′-Chloro-2′-(3-hydroxypropoxy)biphenyl-4-ol **(27)***. Obtained from bromoderivative **26** (262 mg, 0.99 mmol) and 4-hydroxyphenylboronic acid (204 mg, 1.5 mmol) in 82 % yield (226 mg). Chromatography: DCM to DCM/EtOAc, 8:2.

*6-Ethoxy-4′-hydroxy-1,1′-biphenyl-3-carbaldehyde **(33)***. Obtained from bromoderivative **32** (750 mg, 3.3 mmol) and 4-hydroxyphenylboronic acid (677 mg, 4.9 mmol) in 68 % yield (544 mg). Chromatography: DCM to DCM/EtOAc, 9:1.

#### 4.1.3. General procedure 3

*Claisen rearrangement. Method A*. Trimethyl aluminium (4 equiv, 2 M in hexanes) was introduced in a flask and cooled at −20 °C. Then, water (1 equiv) was added and the mixture was allowed to warm to rt. The resulting solution was then cooled to −20 °C prior to the addition of a solution of the proper allyl phenyl ether (1 equiv) in dry DCM (1.7 mL/mmol) and the reaction was stirred at that temperature for 3 h. The crude was diluted with DCM, washed with water and brine, dried ($Na_2SO_4$), filtered, and evaporated under reduced pressure. The residue was purified by chromatography (hexane to hexane/EtOAc 9:1) to yield the corresponding phenol **14.**

*3-Allyl-5′-chloro-2′-ethoxybiphenyl-4-ol **(14)***. Obtained from **13** (85 mg, 0.29 mmol) in 90 % yield (75 mg). Chromatography: hexane to hexane/EtOAc 9:1.

*Method B*. To a solution of the corresponding allyl phenyl ether (1 equiv) in dry DCM (7 mL/mmol) at −20 °C and under an argon atmosphere, diethylaluminium chloride (2.5 equiv, 1 M in hexane) was slowly added and the mixture was allowed to warm to 0 °C and stirred at that temperature for 3 h. The reaction was quenched with 1 M HCl (aq) at 0 °C and the mixture was extracted with EtOAc (2x), washed with brine, dried ($Na_2SO_4$), filtered and evaporated under reduced pressure. The residue was purified by chromatography using the appropriate eluent to afford the corresponding phenols **8**, **23**, **30**, and 2-*O*-ethylhonokiol.

*2′-Ethoxy-3-(allyl)-5′-(propargyl)biphenyl-4-ol **(8)***. Obtained from allyl ether **36** (63 mg, 0.22 mmol) in 51 % yield (33 mg). Chromatography: hexane/EtOAc, 9:1.

*3-Allyl-2′-ethoxy-5′-(3-hydroxypropyl)biphenyl-4-ol **(23)***. Obtained from allyl ether **22** (30 mg, 96 μmol) in 97 % yield (29 mg), and was used in the next step without further purification.

*3,5′-Diallyl-2′-(3-hydroxypropoxy)biphenyl-4-ol **(30)***. Obtained from allyl ether **29** (26 mg, 80 μmol) in 70 % yield (18 mg). Chromatography: hexane to hexane/EtOAc, 6:4.

*3,5′-Diallyl-2′-ethoxybiphenyl-4-ol (2-O-ethylhonokiol)*. Obtained from allyl ether **25** (25 mg, 80 μmol) in 97 % yield (24 mg). Chromatography: hexane to hexane/EtOAc, 9:1.

#### 4.1.4. General procedure 4

*Hydroboration-oxidation of allyl chains.* To a well-stirred solution of the corresponding allyl derivative (1 equiv) in anhydrous THF (2 mL/mmol) at rt, $BH_3$ (2 equiv, 1 M in THF) was added and the mixture was stirred for 4 h. Water was added (0.2 mL/mmol) followed by 3 M NaOH (aq, 0.3 mL/mmol). Then, 30 % $H_2O_2$ (aq, 3.3 mL/mmol) was slowly added at 0 °C and the mixture was stirred at rt for 16 h. The reaction was diluted with EtOAc, washed with water and brine, dried ($Na_2SO_4$), filtered, and evaporated under reduced pressure. The crude was purified by chromatography using the appropriate eluent to afford the corresponding primary alcohols **15** and **21.**

*5′-Chloro-2′-ethoxy-3-(3-hydroxypropyl)biphenyl-4-ol **(15)***. Obtained from allyl derivative **14** (1.19 g, 4.1 mmol) in 84 % yield (1.06 g). Chromatography: hexane to hexane/EtOAc, 7:3.

*2′-Ethoxy-5′-(3-hydroxypropyl)biphenyl-4-ol **(21)***. Obtained from allyl derivative **20** (400 mg, 1.6 mmol) in 53 % yield (227 mg). Chromatography: hexane to hexane/EtOAc, 6:4.

#### 4.1.5. General procedure 5

*Miyaura borylation.* A suspension of the corresponding chloroderivative (1 equiv), $B_2pin_2$ (1.5 equiv), $Pd_2dba_3$ (0.05 equiv), S–PHOS (0.2 equiv), and KOAc (3 equiv), in anhydrous 1,4-dioxane (2 mL/mmol) was heated under an argon atmosphere at 140 °C for 45 min under MW irradiation. Once at rt, the mixture was filtered through a pad of Celite, washed with EtOAc and the solvents were evaporated under reduced pressure. The residue was purified by chromatography using the appropriate eluent to afford the corresponding boronates **16, 19,** and **28**.

*2′-Ethoxy-3-(3-hydroxypropyl)-5′-(4,4,5,5-tetramethyl-1,3,2-dioxaborolan*-2-yl*)-biphenyl-4-ol **(16)***. Obtained from chloroderivative **15** (800 mg, 2.6 mmol) in 89 % yield (929 mg). Chromatography: DCM to DCM/EtOAc, 9:1.

*2′-Ethoxy-5′-(4,4,5,5-tetramethyl-1,3,2-dioxaborolan*-2-yl*)biphenyl-4-ol **(19)***. Obtained from chloroderivative **12** (460 mg, 1.8 mmol) in 75 % yield (472 mg). Chromatography: hexane to hexane/EtOAc, 8:2.

*2′-(3-Hydroxypropoxy)-5′-(4,4,5,5-tetramethyl-1,3,2-dioxaborolan*-2-yl*)biphenyl-4-ol **(28)***. Obtained from chloroderivative **27** (625 mg, 2.5 mmol) in 78 % yield (710 mg). Chromatography: DCM to DCM/EtOH, 98:2.

#### 4.1.6. General procedure 6

*Suzuki coupling of boronates with allyl bromide.* A suspension of the corresponding boronate (1 equiv), allyl bromide (1.2 equiv), $Pd_2dba_3$ (0.24 equiv), and $K_2CO_3$ (6 equiv) in anhydrous toluene (9 mL/mmol of boronate) under an argon atmosphere, was heated at 150 °C for 45 min under MW irradiation. The mixture was filtered through a pad of Celite, washed with EtOAc, and the solvents were evaporated under reduced pressure. The residue was purified by chromatography using the appropriate eluent to afford the corresponding allyl arenes **17**, **20**, and **29**.

*5′-Allyl-2′-ethoxy-3-(3-hydroxypropyl)biphenyl-4-ol **(17)***. Obtained from boronate **16** (247 mg, 0.62 mmol) in 60 % yield (116 mg). Chromatography: DCM to DCM/EtOAc, 9:1.

*5′-Allyl-2′-ethoxybiphenyl-4-ol **(20)***. Obtained from boronate **19** (536 mg, 1.6 mmol) in 75 % yield (301 mg). Chromatography: hexane to hexane/EtOAc, 9:1.

*3-{[5-Allyl-4′-(allyloxy)biphenyl*-2-yl*]oxy}propan-1-ol **(29)***. Obtained from boronate **28** (100 mg, 0.27 mmol), allyl bromide (70 μL, 0.69 mmol) in 47 % yield (41 mg), Chromatography: DCM to DCM/EtOAc 98:2.

#### 4.1.7. General procedure 7

*Activation of alcohols as mesylates.* To a well-stirred solution of the corresponding alcohol (1 equiv) in dry DCM (9.5 mL/mmol) at −20 °C and under an argon atmosphere, methanesulfonyl chloride (MsCl, 1.05 equiv) and anhydrous pyridine (4.2 equiv) were added. The reaction mixture was allowed to warm to rt and stirred for 16 h. Then, concentrated HCl was carefully added and the resulting solution was extracted with EtOAc (2x). The combined organic extracts were sequentially washed with saturated $CuSO_4$ (aq) and brine, dried ($Na_2SO_4$), filtered, and evaporated under reduced pressure. The residue was purified by chromatography using DCM to DCM/EtOAc, 99:1 as eluent to afford the corresponding mesylates **18**, **24**, and **31**.

*3-(5′-Allyl-2′-ethoxy-4-hydroxybiphenyl*-3-yl*)propyl methanesulfonate*

***(18)***. Obtained from alcohol **17** (210 mg, 0.67 mmol) in 42 % yield (110 mg).

*3-(3′-Allyl-6-ethoxy-4′-hydroxybiphenyl-3-yl)propyl methanesulfonate **(24)***. Obtained from alcohol **23** (330 mg, 1.1 mmol) in 77 % yield (319 mg).

*3-[(3′,5-Diallyl-4′-hydroxybiphenyl-2-yl)oxy]propyl methanesulfonate **(31)***. Obtained from alcohol **30** (58 mg, 0.18 mmol) in 53 % yield (38 mg).

#### 4.1.8. General procedure 8

*Nucleophilic substitution of mesylates with $NaN_3$.* To a solution of the corresponding mesylate (1 equiv) in anhydrous DMF (6 mL/mmol) under an argon atmosphere, $NaN_3$ (2 equiv) was added and the reaction mixture was stirred at 60 °C for 16 h. The resulting solution was diluted with EtOAc, washed with water and brine, dried ($Na_2SO_4$), filtered, and evaporated under reduced pressure. The residue was purified by chromatography using the appropriate eluent to afford the corresponding azides **5**, **6**, and **7.**

*5′-Allyl-3-(3-azidopropyl)-2′-ethoxybiphenyl-4-ol **(5)***. Obtained from mesylate **18** (12 mg, 31 μmol) in 70 % yield (7 mg). Chromatography: DCM to DCM/EtOAc, 95:5.

*3-Allyl-5′-(3-azidopropyl)-2′-ethoxybiphenyl-4-ol **(6)***. Obtained from mesylate **24** (260 mg, 0.67 mmol) in 67 % yield (152 mg). Chromatography: hexane to hexane/EtOAc, 9:1.

*3,5′-Diallyl-2′-(3-azidopropoxy)biphenyl-4-ol **(7)***. Obtained from mesylate **31** (41 mg, 0.10 mmol) in 77 % yield (26 mg). Chromatography: hexane to hexane/EtOAc, 9:1.

#### 4.1.9. 1-[4′-(Allyloxy)-6-ethoxy-1,1′-biphenyl-3-yl]propargyl-1-ol **(35)**

To a solution of aldehyde **34** (390 mg, 1.4 mmol) in anhydrous THF (1 mL) at 0 °C and under an argon atmosphere, ethynylmagnesium bromide (8.3 mL, 0.5 M in THF) was added dropwise and the mixture was stirred at rt for 2.5 h. The reaction was quenched with saturated $NH_4Cl$ (aq) at 0 °C, followed by $Et_2O$ and 1 M HCl (aq). The organic phase was separated and the aqueous phase was extracted with $Et_2O$. The combined organic extracts were washed with water and brine, dried ($Na_2SO_4$), filtered and evaporated under reduced pressure to yield pure **35** (412 mg, 97 %), which was used in the next step without further purification.

#### 4.1.10. 2-Ethoxy-4′-(allyloxy)-5-(propargyl)biphenyl **(36)**

To a solution of alcohol **35** (50 mg, 0.16 mmol) in dry DCM (0.4 mL) at 0 °C and under an argon atmosphere, triethylsilane (39 μL, 0.24 mmol) and TFA (50 μL, 0.65 mmol) were added and the mixture was stirred at that temperature for 10 min. The reaction was quenched with saturated $NaHCO_3$ (aq), extracted with DCM, dried ($Na_2SO_4$), filtered, and evaporated under reduced pressure. The crude was purified by chromatography (hexane/EtOAc 8:2 to hexane/EtOAc 7:3) to afford **36** (16 mg, 33 %).

#### 4.1.11. General procedure 9

*Synthesis of amides. Method A.* A suspension of biotin (293 mg, 1.2 mmol), HOBt (163 mg, 1.2 mmol), and activated 4 Å molecular sieves in anhydrous DMF (10 mL) under an argon atmosphere, was heated at 77 °C for 50 min until dissolution of biotin. After cooling to rt, a solution of DCC (272 mg, 1.3 mmol) in dry DCM (2 mL) was added dropwise. The mixture was stirred at rt for 3 h before a solution of 4,4′-diaminobenzophenone (500 mg, 2.4 mmol) and DMAP (15 mg, 0.12 mmol) in anhydrous DMF (2 mL) was added. The resulting mixture was heated at 60 °C for 4 h and allowed to stir at rt for 16 h. The mixture was filtered, washed with DCM/MeOH 1:1, and evaporated under reduced pressure. The crude was purified by chromatography (DCM to DCM/MeOH 7:3) to afford the corresponding amine **37** (500 mg, 97 %).

*Method B.* To a solution of the corresponding carboxylic acid (1 equiv) and HOBt (1.1 equiv) in dry DCM (28 mL/mmol of acid) under an argon atmosphere, EDC (1.1 equiv) was added and the mixture was stirred at rt for 40 min. Then, a solution of the corresponding amine (1.5 equiv) in DMF (4.5 mL/mmol) was added, and the mixture was stirred at rt for 48 h. The reaction was diluted with EtOAc, washed with saturated $NaHCO_3$ (aq), dried ($Na_2SO_4$), filtered, and evaporated under reduced pressure. The crude was purified by chromatography (DCM to DCM/MeOH, 8:2) to afford the corresponding amides **39** and **40**.

*(+)-N-{4-[4-(Biotinylamino)benzoyl]phenyl}hex-5-ynamide **(39)***. Obtained from 5-hexynoic acid (0.25 mL, 2.1 mmol) and amine **37** (578 mg, 1.1 mmol) in 36 % yield (211 mg).

*6-Azido-N-{[(4-biotinylamino)benzoyl]phenyl}hexanamide **(40)***. Obtained from acid **38** (181 mg, 1.2 mmol) and amine **37** (420 mg, 0.96 mmol) in 14 % yield (78 mg).

#### 4.1.12. General procedure 10

*Staudinger reaction to afford amines.* To a solution of the corresponding azide (1 equiv) in anhydrous THF (7.8 mL/mmol) under a nitrogen atmosphere, $PPh_3$ (3 equiv) was added followed by water (10 equiv) and the resulting solution was heated under reflux for 3 h. The solvents were evaporated under reduced pressure and the residue was purified by chromatography (DCM to DCM/MeOH 8:2) to yield the corresponding amines **41** and **42.**

*5′-Allyl-3-(3-aminopropyl)-2′-ethoxybiphenyl-4-ol **(41)***. Obtained from azide **5** (22 mg, 64 μmol) in 76 % yield (15 mg).

*3-Allyl-5′-(3-aminopropyl)-2′-ethoxybiphenyl-4-ol **(42)***. Obtained from azide **6** (40 mg, 0.12 mmol) in 49 % yield (18 mg)

#### 4.1.13. General procedure 11

*Synthesis of probes **1**–**4**.* To a mixture of the corresponding biotinylated alkyne or azide **39** or **40** (1 equiv), $CuSO_4{\cdot}5H_2O$ (1.1 equiv) and sodium ascorbate (1.1 equiv) in water (11 mL/mmol), a solution of the corresponding honokiol-based azide **5**–**7** or alkyne **8** (1 equiv) in DMF (9 mL/mmmol) was added, and the mixture was stirred at rt for 16 h. Then, EtOAc and water were added and the organic phase was separated, washed with brine, dried ($Na_2SO_4$), filtered and evaporated under reduced pressure. The resulting solid was triturated and washed with $Et_2O$ to afford the corresponding pure 1,2,3-triazoles **1**–**4**.

*(+)-N-(4-{4-[(4-{1-[3-(5′-Allyl-2′-ethoxy-4-hydroxybiphenyl-3-yl)propyl]-1H-1,2,3-triazol-4-yl}butanoyl)amino]benzoyl}phenyl)biotinamide **(1)***. Obtained from alkyne **39** (24 mg, 45 μmol) and azide **5** (15 mg, 45 μmol) in 64 % yield (25 mg). Mp: 198.6–199.3 °C. $[\alpha]_D^{20}$:+25.6 (c = 0.18, DMSO). $R_f$: 0.15 (DCM/MeOH, 9:1). IR (ATR, $\nu$): 3300 (OH, NH), 1676 (CO), 1592, 1524, 1474, 1456 (Ar), 1255 (COC); $^1$H NMR (700 MHz, $(CD_3)_2SO$, δ): 1.22 (t, $J$ = 6.9, 3H, $CH_3$), 1.34–1.43 (m, 2H, $C\underline{H}_2CH_2CHS$), 1.48–1.54 (m, 1H, ½$C\underline{H}_2CHS$), 1.60–1.68 (m, 3H, ½$C\underline{H}_2CHS$, $C\underline{H}_2(CH_2)_2CHS$), 1.93 (qt, $J$ = 7.5, 2H, $C\underline{H}_2CH_2C$ = ), 2.09 (qt, $J$ = 7.3, 2H, $C\underline{H}_2CH_2C_3$), 2.37 (td, $J$ = 7.4, 2.6, 2H, $CH_2CO$), 2.42 (t, $J$ = 7.5, 2H, $CH_2CO$), 2.55 (app t, $J$ = 7.5, 2H, $CH_2C_3$), 2.58 (d, $J$ = 12.6, 1H, ½$CH_2S$), 2.67 (t, $J$ = 7.5, 2H, $CH_2C$ = ), 2.83 (dd, $J$ = 12.5, 5.1, 1H, ½$CH_2S$), 3.11–3.14 (m, 1H, CHS), 3.31 (d, $J$ = 6.7, 2H, $CH_2C_5{\cdot}$), 3.96 (q, $J$ = 6.9, 2H, $CH_2O$), 4.14–4.15 (m, 1H, CHN), 4.31 (dd, $J$ = 7.2, 5.5, 1H, CHN), 4.34 (t, $J$ = 7.1, 2H, $CH_2N$), 5.00–5.02 (m, 1H, ½$CH_2$ = ), 5.06 (ddd, $J$ = 17.0, 3.2, 1.4, 1H, ½$CH_2$ = ), 5.95 (ddt, $J$ = 17.0, 10.1, 6.9, 1H, CH = ), 6.37 (br s, 1H, NH), 6.45 (br s, 1H, NH), 6.81 (d, $J$ = 8.2, 1H, $H_5$), 6.95 (d, $J$ = 8.4, 1H, $H_{3'}$), 7.03 (dd, $J$ = 8.2, 2.0, 1H, $H_{4'}$), 7.05 (d, $J$ = 2.0, 1H, $H_{6'}$), 7.15 (dd, $J$ = 8.2, 2.1, 1H, $H_6$), 7.23 (d, $J$ = 2.0, 1H, $H_2$), 7.69 (dd, $J$ = 8.7, 2.0, 4H, $4CH_{Ar}CCO$), 7.75 (dd, $J$ = 8.6, 2.8, 4H, $4CH_{Ar}CN$), 7.92 (s, 1H, NCH = ), 9.41 (br s, 1H, OH), 10.25 (br s, 1H, $NHC_{Ar}$), 10.26 (br s, 1H, $NHC_{Ar}$); $^{13}$C NMR (175 MHz, $(CD_3)_2SO$, δ): 14.7 ($CH_3$), 24.6 ($\underline{C}H_2C$ = ), 24.8 ($\underline{C}H_2CH_2C$ = ), 25.0 ($\underline{C}H_2(CH_2)_2CHS$), 26.8 ($\underline{C}H_2C_3$), 28.1, 28.2 ($(\underline{C}H_2)_2CHS$), 30.1 ($\underline{C}H_2CH_2C_3$), 35.9, 36.4 ($2\underline{C}H_2CO$), 38.7 ($\underline{C}H_2C_5{\cdot}$), 40.0 ($CH_2S$), 49.1 ($CH_2N$), 55.4 (CHS), 59.2, 61.1 (2CHN), 63.5 ($CH_2O$), 112.9 ($C_{3'}$), 114.5 ($C_5$), 115.5 ($CH_2$ = ), 118.2 ($4\underline{C}H_{Ar}CN$), 121.8 (NCH = ), 126.2 ($C_3$), 127.6 ($C_{4'}$), 127.9 ($C_6$), 128.9 ($C_1$), 129.9 ($C_{1'}$), 130.2 ($C_{6'}$), 130.88 ($C_2$), 130.91 ($4\underline{C}H_{Ar}CCO$), 131.7 ($2C_{Ar}N$), 131.8 ($C_{5'}$), 138.2 (CH = ), 143.1 ($2\underline{C}_{Ar}CO$), 146.3 (NC = ), 153.7 ($C_{2'}$), 154.1 ($C_4$), 162.7 (NCON), 171.6, 171.8 (2CON), 193.4

(CO); HRMS (MALDI, *m/z*): calcd for $[M+H]^+$ $C_{49}H_{56}N_7O_6S$: 870.4013; found: 870.4024; HPLC-MS (ESI, *m/z*): 868.4 $[M-H]^-$; $t_R$ (method B): 12.04 min.

*(+)-N-(4-{4-[(4-{1-[3-(3′-Allyl-6-ethoxy-4′-hydroxybiphenyl*-3-yl*)propyl]-1H-1,2,3-triazol*-4-yl*}butanoyl)amino]benzoyl}phenyl)biotinamide* ***(2)***. Obtained from alkyne **39** (79 mg, 0.15 mmol) and azide **6** (50 mg, 0.15 mmol) in 25 % yield (33 mg). Mp: 180.9–181.7 °C. $[\alpha]_D^{20}$:+11.8 (c = 0.39, DMSO). *Rf*: 0.17 (DCM/MeOH, 9:1). IR (ATR, *ν*): 3334 (OH, NH), 1685 (CO), 1596, 1456 (Ar), 1262 (COC); $^1$H NMR (700 MHz, $(CD_3)_2SO$, δ): 1.24 (t, *J* = 6.9, 3H, $CH_3$), 1.24–1.41 (m, 2H, $CH_2CH_2CHS$), 1.48–1.54 (m, 1H, ½$CH_2$CHS), 1.60–1.68 (m, 3H, ½$CH_2$CHS, $CH_2(CH_2)_2$CHS), 1.93 (qt, *J* = 7.4, 2H, $CH_2CH_2C$ = ), 2.10 (qt, *J* = 7.3, 2H, $CH_2CH_2C_3$), 2.37 (td, *J* = 7.3, 2.6, 2H, $CH_2CO$), 2.42 (t, *J* = 7.4, 2H, $CH_2CO$), 2.50–2.53 (m, 2H, $CH_2C_3$), 2.58 (d, *J* = 12.6, 1H, ½$CH_2S$), 2.67 (t, *J* = 7.4, 2H, $CH_2C$ = ), 2.83 (dd, *J* = 12.4, 5.1, 1H, ½$CH_2S$), 3.11–3.14 (m, 1H, CHS), 3.30 (d, *J* = 6.7, 2H, $CH_2C_3$·), 3.95 (q, *J* = 6.9, 2H, $CH_2O$), 4.13–4.15 (m, 1H, CHN), 4.30 (t, *J* = 7.0, 2H, $CH_2N$), 4.29–4.31 (m, 1H, CHN), 4.99–5.01 (m, 1H, ½$CH_2$ = ), 5.06 (ddd, *J* = 17.1, 3.2, 1.5, 1H, ½$CH_2$ = ), 5.97 (ddt, *J* = 16.9, 10.1, 6.7, 1H, CH = ), 6.37 (br s, 1H, NH), 6.45 (br s, 1H, NH), 6.80 (d, *J* = 8.2, 1H, $H_5$·), 6.93 (d, *J* = 8.1, 1H, $H_5$), 7.04–7.06 (m, 2H, $H_2$, $H_4$), 7.16 (dd, *J* = 8.2, 2.0, 1H, $H_6$·), 7.24 (d, *J* = 1.6, 1H, $H_2$·), 7.69 (dd, *J* = 8.6, 1.7, 4H, $4CH_{Ar}CCO$), 7.75 (dd, *J* = 8.6, 3.0, 4H, $4CH_{Ar}CN$), 7.92 (s, 1H, NCH = ), 9.37 (br s, 1H, OH), 10.25 (br s, 1H, $NHC_{Ar}$), 10.26 (br s, 1H, $NHC_{Ar}$); $^{13}$C NMR (175 MHz, $(CD_3)_2SO$, δ): 14.7 ($CH_3$), 24.6 ($CH_2C$ = ), 24.8 ($CH_2CH_2C$ = ), 25.0 ($CH_2(CH_2)_2CHS$), 28.1, 28.2 (($CH_2)_2CHS$), 31.1 ($CH_2C_3$), 31.6 ($CH_2CH_2C_3$), 33.8 ($CH_2C_3$·), 35.9, 36.3 (2$CH_2CO$), 40.0 ($CH_2S$), 48.7 ($CH_2N$), 55.4 (CHS), 59.2, 61.0 (2CHN), 63.5 ($CH_2O$), 112.9 ($C_5$), 114.4 ($C_5$·), 115.3 ($CH_2$ = ), 118.2 (4$CH_{Ar}CN$), 121.9 (NCH = ), 125.2 ($C_3$·), 127.5 ($C_4$), 127.8 ($C_6$·), 128.8 ($C_1$·), 129.9 ($C_1$), 130.0 ($C_2$), 130.8 ($C_2$·), 130.9 (4$CH_{Ar}CCO$), 131.7 (2$C_{Ar}N$), 132.8 ($C_3$), 137.2 (CH = ), 143.1 (2$C_{Ar}CO$), 146.4 (NC = ), 153.6 ($C_6$), 153.9 ($C_4$·), 162.7 (NCON), 171.5, 171.8 (2CON), 193.4 (CO); HRMS (MALDI, *m/z*): calcd for $[M+H]^+$ $C_{49}H_{56}N_7O_6S$: 870.4013; found: 870.3966; HPLC-MS (ESI, *m/z*): 868.3 $[M-H]^-$; $t_R$ (method B): 11.89 min.

*N-[4-(4-{[4-(1-{3-[(3′,5-Diallyl-4′-hydroxybiphenyl*-2-yl*)oxy]propyl}-1H-1,2,3-triazol*-4-yl*)butanoyl]amino}benzoyl)phenyl]biotinamide* ***(3)***. Obtained from alkyne **39** (20 mg, 37 μmol) and azide **7** (13 mg, 37 μmol) in 25 % yield (8 mg). *Rf*: 0.13 (DCM/MeOH, 9:1). IR (ATR, *ν*): 3333 (OH, NH), 1682 (CO), 1591, 1530, 1460 (Ar), 1265 (COC); $^1$H NMR (700 MHz, $(CD_3)_2SO$, δ): 1.35–1.42 (m, 2H, $CH_2CH_2CHS$), 1.49–1.53 (m, 1H, ½$CH_2$CHS), 1.60–1.67 (m, 3H, ½$CH_2$CHS, $CH_2(CH_2)_2$CHS), 1.91 (qt, *J* = 7.5, 2H, $CH_2CH_2C$ = ), 2.16 (qt, *J* = 6.3, 2H, $CH_2CH_2O$), 2.37 (td, *J* = 7.3, 2.8, 2H, $CH_2CO$), 2.41 (t, *J* = 7.6, 2H, $CH_2CO$), 2.58 (d, *J* = 12.7, 1H, ½$CH_2S$), 2.65 (t, *J* = 7.5, 2H, $CH_2C$ = ), 2.83 (dd, *J* = 12.4, 5.1, 1H, ½$CH_2S$), 3.11–3.14 (m, 1H, CHS), 3.31–3.33 (m, 4H, $CH_2C_5$, $CH_2C_3$·), 3.87 (t, *J* = 5.9, 2H, $CH_2O$), 4.13–4.15 (m, 1H, CHN), 4.31 (dd, *J* = 7.5, 5.5, 1H, CHN) 4.38 (t, *J* = 7.0, 2H, $CH_2N$), 4.94–4.95 (m, 1H, ½$CH_2$═$CHCH_2C_3$·), 5.00–5.04 (m, 2H, ½$CH_2$═$CHCH_2C_5$, ½$CH_2$═$CHCH_2C_3$·), 5.06 (ddd, *J* = 16.9, 2.8, 1.5, 1H, ½$CH_2$═$CHCH_2C_5$), 5.92–5.98 (m, 2H, 2CH = ), 6.37 (br s, 1H, NH), 6.45 (br s, 1H, NH), 6.84 (d, *J* = 8.3, 1H, $H_5$·), 6.94 (d, *J* = 8.2, 1H, $H_3$), 7.03 (dd, *J* = 8.3, 2.2, 1H, $H_4$), 7.04 (d, *J* = 2.1, 1H, $H_6$), 7.17 (dd, *J* = 8.2, 2.1, 1H, $H_6$·), 7.25 (d, *J* = 1.9, 1H, $H_2$·), 7.69 (d, *J* = 8.6, 4H, $4CH_{Ar}CCO$), 7.76 (d, *J* = 9.7, 4H, $4CH_{Ar}CN$), 7.77 (s, 1H, NCH = ), 9.42 (br s, 1H, OH), 10.25 (br s, 1H, $NHC_{Ar}$), 10.26 (br s, 1H, $NHC_{Ar}$); $^{13}$C NMR (175 MHz, $(CD_3)_2SO$, δ): 24.6 ($CH_2C$ = ), 24.8 ($CH_2CH_2C$ = ), 25.0 ($CH_2(CH_2)_2CHS$), 28.1, 28.2 (($CH_2)_2CHS$), 29.6 ($CH_2CH_2O$), 33.8 ($CH_2C_3$·), 35.9, 36.3 (2$CH_2CO$), 38.7 ($CH_2C_5$), 40.0 ($CH_2S$), 46.3 ($CH_2N$), 55.4 (CHS), 59.2, 61.0 (2CHN), 64.7 ($CH_2O$), 112.9 ($C_3$), 114.5 ($C_5$·), 115.3, 115.5 (2$CH_2$ = ), 118.2 (4$CH_{Ar}CN$), 121.9 (NCH = ), 125.4 ($C_3$·), 127.7 ($C_4$), 127.9 ($C_6$·), 128.8 ($C_1$·), 130.16 ($C_1$), 130.21 ($C_6$), 130.7 ($C_2$), 130.9 (4$CH_{Ar}CCO$), 131.7 (2$C_{Ar}N$, $C_5$), 137.2 ($CHCH_2C_3$·), 138.1 ($CHCH_2C_5$), 143.1 (2$C_{Ar}CO$), 146.4 (NC = ), 153.4 ($C_2$), 154.0 ($C_4$·), 162.7 (NCON), 171.5, 171.8 (2CON), 193.4 (CO); HRMS (ESI, *m/z*): calcd for $[M-H]^-$ $C_{50}H_{54}N_7O_6S$: 880.3862; found: 880.3844; HPLC-MS (ESI, *m/z*): 880.4 $[M-H]^-$; $t_R$ (method B): 12.54 min.

*(+)-6-(4-{[6-Ethoxy-4′-hydroxy-3′-(allyl)biphenyl*-3-yl*]methyl}-1H-1,2,3-triazol*-1-yl*)-N-biotinylamino)benzoyl]phenyl}hexanamide* ***(4)***. Obtained from azide **40** (26 mg, 44 μmol) and alkyne **8** (13 mg, 44 μmol) in 49 % yield (19 mg). Mp: 143–146 °C. $[\alpha]_D^{20}$:+27.8 (c = 0.23, DMSO). *Rf*: 0.12 (DCM/MeOH, 9:1). IR (ATR, *ν*): 3305 (OH, NH), 1688, 1593 (CO), 1525, 1459, 1405 (Ar), 1259 (COC); $^1$H NMR (700 MHz, $(CD_3)_2SO$, δ): 1.23 (t, *J* = 6.9, 3H, $CH_3$), 1.25–1.28 (m, 2H, $CH_2(CH_2)_2N$), 1.35–1.46 (m, 2H, $CH_2CH_2CHS$), 1.48–1.53 (m, 1H, ½$CH_2CHS$), 1.59–1.68 (m, 5H, ½$CH_2CHS$, $CH_2(CH_2)_2CHS$, $CH_2(CH_2)_3N$), 1.81 (qt, *J* = 7.3, 2H, $CH_2CH_2N$), 2.33 (t, *J* = 7.4, 2H, $CH_2CO$), 2.35–2.38 (m, 2H, $CH_2CO$), 2.58 (d, *J* = 12.5, 1H, ½$CH_2S$), 2.82 (dd, *J* = 12.4, 5.1, 1H, ½$CH_2S$), 3.11–3.14 (m, 1H, CHS), 3.30 (d, *J* = 6.6, 2H, $CH_2C_3$·), 3.91 (s, 2H, $CH_2C_3$) 3.94 (q, *J* = 7.0, 2H, $CH_2O$), 4.13–4.15 (m, 1H, CHN), 4.28–4.32 (m, 3H, CHN, $CH_2N$), 5.00 (br d, *J* = 9.9, 1H, ½$CH_2$ = ), 5.07 (dd, *J* = 17.1, 1.3, 1H, ½$CH_2$ = ), 5.96 (ddt, *J* = 17.0, 10.1, 6.8, 1H, CH = ), 6.37 (br s, 1H, NH), 6.45 (br s, 1H, NH), 6.80 (d, *J* = 8.2, 1H, $H_5$·), 6.93 (d, *J* = 8.4, 1H, $H_5$), 7.06 (dd, *J* = 8.40, 2.0, 1H, $H_4$), 7.10 (d, *J* = 1.9, 1H, $H_2$), 7.12 (dd, *J* = 8.3, 2.0, 1H, $H_6$·), 7.20 (d, *J* = 1.6, 1H, $H_2$·), 7.69 (d, *J* = 8.6, 4H, $4CH_{Ar}CCO$), 7.74 (d, *J* = 8.0, 2H, $2CH_{Ar}CN$), 7.76 (d, *J* = 8.4, 2H, $2CH_{Ar}CN$), 7.83 (m, 1H, NCH = ), 9.39 (br s, 1H, OH), 10.23 (br s, 1H, $NHC_{Ar}$), 10.25 (br s, 1H, $NHC_{Ar}$); $^{13}$C NMR (175 MHz, $(CD_3)_2SO$, δ): 14.7 ($CH_3$), 24.4, 25.0, 25.5 ($CH_2(CH_2)_2CHS$, ($CH_2)_2CH_2CO$), 28.1, 28.2 (($CH_2)_2CHS$), 29.6 ($CH_2CH_2N$), 30.5 ($CH_2C_3$), 33.8 ($CH_2C_3$·), 36.3, 36.4 (2$CH_2CO$), 40.0 ($CH_2S$), 49.0 ($CH_2N$), 55.4 (CHS), 59.2, 61.1 (2CHN), 63.5 ($CH_2O$), 112.9 ($C_5$), 114.4 ($C_5$·), 115.4 ($CH_2$ = ), 118.2 (4$CH_{Ar}CN$), 122.2 (NCH = ), 125.2 ($C_3$·), 127.7 ($C_4$), 127.8 ($C_6$·), 128.8 ($C_1$·), 129.9 ($C_1$), 130.2 ($C_2$), 130.7 ($C_2$·), 130.9 (4$CH_{Ar}CCO$), 131.7 (2$C_{Ar}N$), 131.8 ($C_3$), 137.1 (CH = ), 143.1 (2$C_{Ar}CO$), 146.5 (NC = ), 153.7 ($C_6$), 153.9 ($C_4$·), 162.7 (NCON), 171.7, 171.8 (2CON), 193.4 (CO); HRMS (MALDI, *m/z*): calcd for $[M+H]^+$ $C_{49}H_{56}N_7O_6S$: 870.4013; found: 870.4027; HPLC-MS (ESI, *m/z*): 868.4 $[M-H]^-$; $t_R$ (method B): 11.21 min.

#### 4.1.14. General procedure 12

*Synthesis of probes* ***9,10***. To a solution of acid **43** (1 equiv) in dry DCM (6.7 mL/mmol of acid), HOBt (1.2 equiv) was added under a nitrogen atmosphere and the mixture was stirred at rt for 10 min. Then, a solution of EDC (1.2 equiv) in dry DCM (6.7 mL/mmol of acid) was added and the reaction was stirred at rt for 30 min before a solution of the corresponding amine **41** or **42** (1 equiv) in dry DCM (6.7 mL/mmol of amine) was added, followed by DIPEA (2.2 equiv). The resulting mixture was stirred at rt for 16 h, diluted with EtOAc, washed with saturated $NaHCO_3$ (aq, 2x) and brine. The organic layer was dried ($Na_2SO_4$), filtered, and evaporated under reduced pressure. The residue was purified by chromatography (DCM to DCM/EtOAc, 95:5) to afford the corresponding amides **9** and **10**.

*N-[3-(5′-Allyl-2′-ethoxy-4-hydroxybiphenyl*-3-yl*)propyl]-3-(3-but-3-yn*-1-yl-*3H-diaziren*-3-yl*)propanamide* ***(9)***. Obtained from acid **43** (5 mg, 30 μmol) and amine **41** (9 mg, 30 μmol) in 45 % yield (6 mg). *Rf*: 0.07 (DCM/EtOAc, 95:5). IR (ATR, *ν*): 3305, 3367 (NH, OH), 1644 (CO), 1550, 1509, 1491, 1469 (Ar), 1271, 1237 (COC); $^1$H NMR (700 MHz, $CD_3OD$, δ): 1.30 (t, *J* = 7.0, 3H, $CH_3$), 1.60 (t, *J* = 7.5, 2H, $CH_2CH_2C$≡), 1.73 (t, *J* = 7.1, 1H, $CH_2CH_2CO$), 1.83 (qt, *J* = 7.4, 2H, $CH_2CH_2C_3$), 1.99 (td, *J* = 7.5, 2.7, 2H, $CH_2C$≡), 2.00 (t, *J* = 7.7, 2H, $CH_2CO$), 2.21 (t, *J* = 2.7, 1H, CH≡), 2.67 (t, *J* = 7.5, 2H, $CH_2C_3$), 3.22 (t, *J* = 7.1, 2H, $CH_2N$), 3.34 (d, *J* = 6.7, 2H, $CH_2C_5$·), 3.97 (q, *J* = 7.0, 2H, $CH_2O$), 5.01–5.03 (m, 1H, ½$CH_2$ = ), 5.06 (ddd, *J* = 17.0, 3.6, 1.7, 1H, ½$CH_2$ = ), 5.97 (ddt, *J* = 17.0, 10.1, 6.8, 1H, CH = ), 6.76 (d, *J* = 8.3, 1H, $H_5$), 6.91 (d, *J* = 8.3, 1H, $H_3$·), 7.03 (dd, *J* = 8.2, 2.2, 1H, $H_4$·), 7.06 (d, *J* = 2.2, 1H, $H_6$·), 7.16 (dd, *J* = 8.2, 2.3, 1H, $H_6$), 7.25 (d, *J* = 2.2, 1H, $H_2$); $^{13}$C NMR (175 MHz, 9:1 $CD_3OD/CDCl_3$, δ): 13.8 ($CH_2C$≡), 15.3 ($CH_3$), 28.7 ($CH_2CH_2CO$), 28.8 ($CN_2$), 29.9 ($CH_2CO$), 30.6 ($CH_2CH_2C_3$), 31.1 ($CH_2CH_2C$≡), 33.3 ($CH_2C_3$), 40.3, 40.4 ($CH_2N$, $CH_2C_5$·), 65.3 ($CH_2O$), 70.2 (CH≡), 83.5

(C≡), 114.3 ($C_{3'}$), 115.3 ($C_5$), 115.6 ($CH_2$ = ), 128.2 ($C_3$), 128.7 ($C_{4'}$), 129.1 ($C_6$), 131.3 ($C_1$), 131.6 ($C_{6'}$), 132.3 ($C_{1'}$), 132.4 ($C_2$), 133.6 ($C_{5'}$), 139.3 (CH = ), 155.2 ($C_4$), 155.4 ($C_{2'}$), 174.2 (CON); HRMS (ESI, *m/z*): calcd for $[M+Na]^+$ $C_{28}H_{33}N_3NaO_3$: 482.2420; found: 482.2414; HPLC-MS (ESI, *m/z*): 458.0 $[M-H]^-$; $t_R$ (method A): 11.07 min.

*N-[3-(3′-Allyl-6-ethoxy-4′-hydroxybiphenyl-3-yl)propyl]-3-(3-but-3-yn-1-yl-3H-diaziren-3-yl)propanamide (**10**).* Obtained from acid **43** (5 mg, 30 μmol) and amine **42** (9 mg, 30 μmol) in 62 % yield (9 mg). Chromatography: DCM to DCM/MeOH 95:5. *Rf*: 0.10 (DCM/EtOAc, 95:5). IR (ATR, *ν*): 3293, 3078 (NH, OH), 1640 (CO), 1607, 1472, 1439 (Ar), 1269, 1235 (COC); $^1$H NMR (700 MHz, $CD_3OD$, δ): 1.29 (t, *J* = 7.0, 3H, $CH_3$), 1.59 (t, *J* = 7.5, 2H, $CH_2CH_2C$≡), 1.72 (t, *J* = 7.2, 2H, $CH_2CH_2CO$), 1.81 (qt, *J* = 7.3, 2H, $CH_2CH_2C_3$), 1.98–2.01 (m, 4H, $CH_2C$≡, $CH_2CO$), 2.22 (t, *J* = 2.6, 1H, CH≡), 2.61 (t, *J* = 7.6, 2H, $CH_2C_3$), 3.18 (t, *J* = 7.0, 2H, $CH_2N$), 3.38 (d, *J* = 6.6, 2H, $CH_2C_{3'}$), 3.95 (q, *J* = 7.0, 2H, $CH_2O$), 4.99–5.01 (m, 1H, ½$CH_2$ = ), 5.06 (ddd, *J* = 17.1, 3.5, 1.6, 1H, ½$CH_2$ = ), 6.02 (ddt, *J* = 16.9, 10.2, 6.7, 1H, CH = ), 6.78 (d, *J* = 8.2, 1H, $H_{5'}$), 6.89 (d, *J* = 8.3, 1H, $H_5$), 7.04 (dd, *J* = 8.3, 2.2, 1H, $H_4$), 7.08 (d, *J* = 2.2, 1H, $H_2$), 7.18 (dd, *J* = 8.2, 2.2, 1H, $H_{6'}$), 7.25 (d, *J* = 2.1, 1H, $H_{2'}$); $^{13}$C NMR (175 MHz, 9:1 $CD_3OD/CDCl_3$ δ): 13.8 ($CH_2C$≡), 15.3 ($CH_3$), 28.8 ($CN_2$), 29.8 ($CH_2CH_2CO$), 31.0 ($CH_2CO$), 32.3 ($CH_2CH_2C_3$), 33.3 ($CH_2CH_2C$≡), 33.4 ($CH_2C_3$), 35.2 ($CH_2C_{3'}$), 40.1 ($CH_2N$), 65.4 ($CH_2O$), 70.2 (CH≡), 83.5 (C≡), 114.3 ($C_5$), 115.3 ($C_{5'}$), 115.4 ($CH_2$ = ), 126.9 ($C_{3'}$), 128.5 ($C_4$), 129.2 ($C_{6'}$), 131.3 ($C_{1'}$), 131.4 ($C_2$), 132.3 ($C_{2'}$, $C_1$), 135.3 ($C_3$), 138.5 (CH = ), 155.0 ($C_{4'}$), 155.3 ($C_6$), 174.2 (CON); HRMS (ESI, *m/z*): calcd for $[M+Na]^+$ $C_{28}H_{33}N_3NaO_3$: 482.2420; found: 482.2401; HPLC-MS (ESI, *m/z*): 458.1 $[M-H]^-$; $t_R$ (method A): 10.64 min.

### 4.2. Cell culture

MDA-MB-231 cells were grown in Dulbecco's modified Eagle medium (DMEM), while SKOV3 and OVCAR3 cells were grown in RPMI-1640 medium, both supplemented with 10 % fetal bovine serum (FBS), 1 % non-essential amino acids, 1 % sodium pyruvate, 100 U/mL penicillin, and 100 μg/mL streptomycin in a 5 % $CO_2$ humidified atmosphere at 37 °C. For passage, cells were rinsed with PBS and incubated with 0.125 % trypsin (0.02 % EDTA solution) at 37 °C for 2 min. Detached cells were resuspended in growth medium, counted if necessary, and split onto fresh dishes.

### 4.3. Cytoxicity assay

Cell viability was assessed by a colorimetric assay based on the metabolic reduction of 3-[4,5-dimethylthiazol-2-yl]-2,5-diphenyltetrazolium bromide (MTT) to formazan by the mitochondrial enzyme succinate dehydrogenase as previously described [101]. Briefly, MDA-MB-231, SKOV3, or OVCAR3 cells were plated in a 96-well plate (7500 cells/well) and treated with 50 μM of compounds under study or with DMSO (vehicle-treated cells) in growth media (100 μL), in a 5 % $CO_2$ humidified atmosphere at 37 °C for 48 h. Then, after removing the culture media, 100 μL of a premixed 2:3 solution of MTT/growth media (5 mg/mL of MTT in PBS) were added to each well, and cells were incubated at 37 °C for 4 h protected from light. The medium was carefully removed and precipitated formazan was dissolved in 100 μL of DMSO and shaken mechanically for 5 min. The absorbance values were measured at a wavelength of 570 nm on a multi-well plate reader (Model Anthos Labtec 2010 1.7). Percentages of cell viability were relative to the DMSO controls. For those compounds that reduced cell viability more than 50 % at 50 μM, full dose-response curves, using concentrations of compounds ranging between 0 and 200 μM, were carried out to determine the $IC_{50}$ value. $IC_{50}$ values were obtained by nonlinear regression (sigmoidal dose-response curve) fitting using GraphPad Prism 10 and they are expressed as the average ± SEM obtained from two independent experiments carried out in triplicate.

### 4.4. In-gel analysis

For in situ labeling, cells were plated in 6 cm dishes and grown to 100 % confluency, washed with PBS, and treated with the corresponding concentration of probe **9** or **10** (0.2–20 μM) in 1 mL of serum-free media. For the competition experiments, 10 μM of probe **9** or **10** and 100 μM of honokiol or 2-*O*-ethylhonokiol were used. After 30 min at 37 °C, media was aspirated off and cells were irradiated (365 nm, 4 °C, 10 min) using a Stratagene UV Stratalinker 1800 and scrapped in 1 mL of cold PBS (pH 7.4). Cell pellets were isolated by centrifugation (3000 rpm, 3 min), rinsed with PBS and centrifuged (3000 rpm, 3 min, 2x), lysed by probe sonication, and centrifuged (100000*g*, 45 min) to provide the soluble (supernatant) and membrane (pellet) fractions. Protein concentrations were determined using the bicinchoninic acid (BCA) protein assay (Bio-Rad) following the manufacturer's instructions, and adjusted to 1 mg/mL. Then, 50 μg of lysate were conjugated to rhodamine azide (Rh–$N_3$) [100] by treating with 6 μL of a pre-mixed solution containing 3 μL of 1.7 mM tris[(1-benzyl-1*H*-1,2,3-triazol-4-yl)methyl]amine (TBTA) in 4:1 DMSO:*t*-BuOH, 1 μL of 50 mM $CuSO_4$ in water, 1 μL of 50 mM tris (2-carboxyethyl)phosphine) (TCEP) in water (freshly prepared), and 1 μL of 1.25 mM Rh–$N_3$ in DMSO. After 1 h at rt in the dark, samples were mixed with Laemmli loading buffer and 30 μL of the click reaction mixture (20 μg of protein) were loaded into each gel lane and resolved using SDS-PAGE. Images were acquired using a Hitachi FMBIO-II flatbed fluorescence scanner. Fluorescent images are shown in grey scale.

### 4.5. Sample processing for SILAC quantitative mass spectrometry

MDA-MB-231 cells, cultured as described above, were plated in 10 cm dishes and grown to 100 % confluency and washed with PBS. "Light" cells were treated with probe **10** (10 μM) and honokiol (100 μM), and "heavy" cells only with probe **10** (10 μM) in 2 mL of serum-free media. Cells were incubated with compound(s) at 37 °C for 30 min, irradiated (365 nm, 4 °C, 10 min), harvested, and lysed as described above. Heavy and light proteomes were combined in equal amounts (0.75 mg of proteome each) and diluted with PBS to a final volume of 1.0 mL. The sample was treated with 110 μL of a pre-mixed solution containing 60 μL of 1.7 mM TBTA in 4:1 DMSO:$^t$BuOH, 20 μL of 50 mM $CuSO_4$ in water, 20 μL of 50 mM TCEP in water (freshly prepared) and 10 μL of 10 mM biotin-$PEG_3$-azide (ChemPepInc). After mixing for 1 h at rt, MeOH (2.0 mL), chloroform (0.5 mL), and PBS (1.0 mL) were added to the reaction mixture and the cloudy mixture was centrifuged at 5000 rpm for 15 min yielding a precipitated protein disc between the aqueous and organic layers. The top and bottom liquid phases were aspirated, and the protein disc was then washed with MeOH:chloroform (1:1 vol, 3x2 mL). MeOH (2 mL) was then added and the solution was sonicated to yield a cloudy mixture. Chloroform (0.5 mL) was added and the solution was centrifuged (5000 rpm, 10 min), aspirated, and the pellet was solubilized in urea (500 μL, 6 M in PBS). The solution was treated with 1:1 vol of TCEP: $K_2CO_3$ (50 μL, 200 mM:600 mM in PBS). The pellet was resuspended by sonication, and the resulting solution was incubated at 37 °C for 30 min. Then, iodoacetamide (70 μL, 400 mM in PBS) was added and the solution was incubated at rt for 30 min in the dark. 10 % SDS in PBS was then added to each sample, followed by 5.5 mL of PBS to achieve a final concentration of 0.2 % SDS. Streptavidin beads (Thermo Fisher) [100 μL slurry previously washed with PBS (3x)] were added and the mixture was rotated at rt for 2 h. Beads were washed with 0.2 % SDS in PBS (5 mL), PBS (2x5 mL), and water (2x5 mL) before transferring to low-bind eppendorf tubes and centrifuged (1000 rpm, 2 min) into a pellet. Following aspiration of the supernatant, the beads were resuspended in 200 μL of urea (2 M in PBS) supplemented with $CaCl_2$ (1.0 mM final concentration) and sequencing grade porcine trypsin (Promega). Following overnight digestion at 37 °C, the tryptic digest solution (supernatant) was removed from the beads following centrifugation (1000 rpm, 2 min) and acidified with 5 % formic acid. The tryptic digests were stored at −20 °C until analyzed by LC-MS/MS.

### 4.6. Mass spectrometry and data analysis

Mass spectrometry was performed using a Thermo Orbitrap Velos mass spectrometer. Peptides were eluted using a five-step multidimensional LC-MS (MudPIT [102]) protocol (using 0 %, 25 %, 50 %, 80 % and 100 % salt bumps of 500 mM aqueous $NH_4OAc$, followed by an increasing gradient of aqueous acetonitrile and 0.1 % formic acid in each step), and data were collected in data-dependent acquisition mode −two MS1 microscans (400–1800 mass to charge ratio [*m/z*]) and 30 data dependent fragmentation (MS2) scans− with dynamic exclusion enabled (repeat count of 1, exclusion duration of 20 s) with monoisotopic precursor selection enabled. All other parameters were left at default values. Prolucid searches allowed for variable oxidation of methionine (+15.9949 *m/z*), static modification of cysteine residues (+57.0215 *m/z*; iodoacetamide alkylation) and accepted only half or fully tryptic peptides. Each data set was independently searched with light and heavy parameter files; for the light search, all other amino acids were left at default masses; for the heavy search, static modifications on lysine (+8.0142 *m/z*) and arginine (+10.0082 *m/z*) were specified. The precursor-ion mass tolerance was set to 50 ppm and the fragment-ion mass tolerance was the default assignment of 0. The data were searched using the human reverse-concatenated nonredundant (gene--centric) FASTA database that assembled from the Uniprot database (www.uniprot.org). The resulting matched MS2 spectra were assembled into protein identifications, then filtered using DTASelect (version 2.0.47), and only half-tryptic or fully tryptic peptides were accepted for identification, and only fully-tryptic peptides were considered for quantification. Peptides were restricted to a specified false positive rate of 1 %. Redundant peptide identifications common between multiple proteins were allowed, but the database was restricted to a single consensus splice variant. SILAC ratios were quantified using in-house software as described (CIMAGE [103]). Briefly, extracted MS1 ion chromatograms (±10 ppm) from both "light" and "heavy" targeted peptide masses (*m/z*) were generated using a retention time window (±10 min) centered on the time when the peptide ion was selected for MS/MS fragmentation, and subsequently identified. Next, the ratio of the peak areas under the light and heavy signals (signal-to-noise ratio>2.5) are calculated. Computational filters used to ensure that the correct peak-pair is used for quantification include a co-elution correlation score filter ($R^2 \geq 0.8$), removing target peptides with bad co-elution profile, and an "envelope correlation score" filter ($R^2 > 0.8$) that eliminates target peptides whose predicted pattern of the isotopic envelope distribution does not match the experimentally observed high-resolution MS1 spectrum. Also peptides detected as singletons, where only the heavy or light isotopically labeled peptide was detected and sequenced −but which passed all other filtering parameters− were given the maximum standard SILAC ratio of 20.

### 4.7. Cellular thermal shift assay (CETSA)

CETSA assay followed by western blotting was carried out as described previously with some modifications [104,105]. Briefly, MDA-MB-231 cells were plated in a P100 (Corning) at a density of $2{\cdot}10^6$ cells/well and cultured for 24 h. Then, cells were incubated with 10 μM honokiol solution or vehicle for 1 h at 37 °C, washed with PBS, detached with trypsin and centrifuged (250*g*, 25 °C, 5 min). The resulting pellet was resuspended in 400 μL of PBS, transferred to PCR tubes (24 μL/tube) and heat-shocked for 3 min at the corresponding temperature (37–61 °C or 37–63 °C) using a SensoQuest LabCycler Thermocycler (Progen Scientific Ltd), followed by rapid cooling to 25 °C. Igepal-630 was then added to the samples (final concentration of 1 % v/v), and the samples were thoroughly mixed and denatured by three cycles of freezing/thawing using liquid nitrogen. The non-soluble fraction was separated by centrifugation (12000*g*, 20 min, 4 °C) and the supernatant was transferred to clean microtubes. Then, Laemmli buffer (Bio-Rad) was added, and samples were heated at 100 °C for 10 min.

For the western-bot analysis, equal amounts of protein were separated by SDS-PAGE and transferred to a nitrocellulose membrane (Amersham Protran 0.45 μm) using a wet tank (100 v for 60 min). The membranes were then blocked for 1 h at rt with Tris-buffered saline with 0.05 % v/v Tween20® (TBST) and 5 % bovine serum albumin (BSA), followed by incubation overnight with the primary antibody (Lyric 1:500, 2F11C3D4 SantaCruz, sc-517220; CAPN-1 1:500, A-5 SantaCruz, sc-390677; PGD 1:500, G-2 SantaCruz, sc-398977; DPP3 1:500, EPR9020(B) Abcam, ab133671) at 4 °C. After that, the primary antibody was removed, the membrane was washed three times with TBST and incubated with the secondary antibody (goat α-Mouse IgG (H + L) HRP Conjugate, 1:10000, Bio-Rad and goat α-Rabbit IgG HRP Conjugate, 1:10000, Bio-Rad) for 1 h at rt. The secondary antibody was removed and membranes were washed six times with TBST and incubated with ECL™ Western Blotting Detection Reagents (Cytiva, Amersham) for 3 min. The luminescence signal was detected using a Universal Hood II ChemiDoc XRS + System (Bio-Rad). Signal intensities were determined by quantification of chemiluminescence counts per square millimeter using the Image-Lab software (Bio-Rad). Signals were normalized with respect to the intensity of the soluble fraction obtained at 37 °C, which was established as 100 % non-denatured protein. Curves were generated and fitted using a four-parameter nonlinear regression curve fit in GraphPad Prism.

## CRediT authorship contribution statement

**Henar Vázquez-Villa:** Writing – review & editing, Investigation, Formal analysis, Data curation. **Ainoa Rueda-Zubiaurre:** Investigation, Formal analysis, Data curation. **Daniel Fernández:** Writing – review & editing, Investigation, Formal analysis, Data curation. **Román Foronda:** Writing – review & editing, Investigation, Formal analysis, Data curation. **Christopher G. Parker:** Writing – review & editing, Supervision, Resources, Investigation. **Benjamin F. Cravatt:** Supervision, Resources, Project administration, Funding acquisition. **Mar Martín-Fontecha:** Writing – review & editing, Visualization, Supervision, Methodology, Formal analysis, Conceptualization. **Silvia Ortega-Gutiérrez:** Writing – review & editing, Writing – original draft, Visualization, Supervision, Project administration, Methodology, Funding acquisition, Conceptualization.

## Declaration of competing interest

The authors declare the following financial interests/personal relationships which may be considered as potential competing interests: Silvia Ortega-Gutierrez reports financial support was provided by Ministerio de Ciencia e Innovacion. Daniel Fernandez reports financial support was provided by Comunidad de Madrid. Benjamin F. Cravatt reports financial support was provided by National Institutes of Health. Roman Foronda reports financial support was provided by Comunidad de Madrid. If there are other authors, they declare that they have no known competing financial interests or personal relationships that could have appeared to influence the work reported in this paper.

## Acknowledgements

This work has been supported by Grant PID2022-138797OB-I00 funded by MCIN/AEI/10.13039/501100011033 and by ERDF A way of making Europe, by Comunidad de Madrid (Predoctoral fellowships PEJ-2020-AI/BMD-18172 and PIPF-2022/SAL-GL-24817 to R.F. and D. F., respectively), and by the National Institutes of Health (grant NIH R35 CA231991). Biorender was used to prepare the graphical abstract and Fig. 2A.

## Appendix A. Supplementary data

Supplementary data to this article can be found online at https://doi.

org/10.1016/j.ejmech.2024.117102.

## Data availability

Data supporting the conclusions of this work are included in the manuscript or in the Supporting Information.

## References


[1] X. Cai, X. Jiang, M. Zhao, K. Su, M. Tang, F. Hong, N. Ye, R. Zhang, N. Li, L. Wang, L. Xue, Z. Zhu, L. Chen, J. Yang, W. Wu, H. Ye, Identification of the target protein and molecular mechanism of honokiol in anti-inflammatory action, Phytomedicine 109 (2023) 154617.

[2] C. Salgado-Benvindo, A.A. Leijs, M. Thaler, A. Tas, J.L. Arbiser, E.J. Snijder, M. J. van Hemert, Honokiol inhibits SARS-CoV-2 replication in cell culture at a post-entry step, Microbiol. Spectr. 11 (2023) e0327322.

[3] C. Ochoa, A.E. Solinski, M. Nowlan, M.M. Dekarske, W.M. Wuest, M. C. Kozlowski, A bisphenolic honokiol analog outcompetes oral antimicrobial agent cetylpyridinium chloride via a membrane-associated mechanism, ACS Infect. Dis. 6 (2020) 74–79.

[4] B. Taferner, W. Schuehly, A. Huefner, I. Baburin, K. Wiesner, G.F. Ecker, S. Hering, Modulation of GABAA-receptors by honokiol and derivatives: subtype selectivity and structure-activity relationship, J. Med. Chem. 54 (2011) 5349–5361.

[5] C.P. Ong, W.L. Lee, Y.Q. Tang, W.H. Yap, Honokiol: a review of its anticancer potential and mechanisms, Cancers 12 (2019) 48.

[6] R. Yang, E. Hou, W. Cheng, X. Yan, T. Zhang, S. Li, H. Yao, J. Liu, Y. Guo, Membrane-targeting neolignan-antimicrobial peptide mimic conjugates to combat methicillin-resistant Staphylococcus aureus (MRSA) infections, J. Med. Chem. 65 (2022) 16879–16892.

[7] R. Yang, L. Cui, T. Xu, Y. Zhong, S. Hu, J. Liu, S. Qin, X. Wang, Y. Guo, Discovery of membrane-targeting amphiphilic honokiol derivatives containing an oxazolethione moiety to combat methicillin-resistant Staphylococcus aureus (MRSA) infections, Eur. J. Med. Chem. 279 (2024) 116868.

[8] Ido Wolf, James O'Kelly, Naoki Wakimoto, Anh Nguyen, Franck Amblard, Beth Y Karlan, Jack L Arbiser, H Phillip Koeffler Honokiol, A natural biphenyl, inhibits in vitro and in vivo growth of breast cancer through induction of apoptosis and cell cycle arrest, Int J Oncol. 30 (6) (2007) 1529–1537.

[9] D. Lin, Z. Yan, A. Chen, J. Ye, A. Hu, J. Liu, J. Peng, X. Wu, Anti-proliferative activity and structure-activity relationship of honokiol derivatives, Bioorg. Med. Chem. 27 (2019) 3729–3734.

[10] M. Zhu, B. Li, H. Ma, X. Huang, H. Wang, Y. Dai, Y. Li, H.M. Li, C.Z. Wu, Synthesis and in vitro antitumor evaluation of honokiol derivatives, Bioorg. Med. Chem. Lett. 30 (2020) 126849.

[11] H. Tang, Y. Zhang, D. Li, S. Fu, M. Tang, L. Wan, K. Chen, Z. Liu, L. Xue, A. Peng, H. Ye, L. Chen, Discovery and synthesis of novel magnolol derivatives with potent anticancer activity in non-small cell lung cancer, Eur. J. Med. Chem. 156 (2018) 190–205.

[12] M. Zhao, Y.H. Zheng, Q.Y. Zhao, W. Zheng, J.H. Yang, H.Y. Pei, L. Liu, K.J. Liu, L. L. Xue, D.X. Deng, L. Wang, X. Ma, S.H. Fu, A.H. Peng, M.H. Tang, Y.Z. Luo, H. Y. Ye, L.J. Chen, Synthesis and evaluation of new compounds bearing 3-(4-aminopiperidin-1-yl)methyl magnolol scaffold as anticancer agents for the treatment of non-small cell lung cancer via targeting autophagy, Eur. J. Med. Chem. 209 (2021) 112922.

[13] K.J. Huang, C.H. Kuo, S.H. Chen, C.Y. Lin, Y.R. Lee, Honokiol inhibits in vitro and in vivo growth of oral squamous cell carcinoma through induction of apoptosis, cell cycle arrest and autophagy, J. Cell Mol. Med. 22 (2018) 1894–1908.

[14] D. Bui, L. Li, T. Yin, X. Wang, S. Gao, M. You, R. Singh, M. Hu, Pharmacokinetic and metabolic profiling of key active components of dietary supplement Magnolia officinalis extract for prevention against oral carcinoma, J. Agric. Food Chem. 68 (2020) 6576–6587.

[15] M. Mei, L. Tang, H. Zhou, N. Xue, M. Li, Honokiol prevents lung metastasis of triple-negative breast cancer by regulating polarization and recruitment of macrophages, Eur. J. Pharmacol. 959 (2023) 176076.

[16] S. Bhukta, P. Gopinath, R. Dandela, Target identification of anticancer natural products using a chemical proteomics approach, RSC Adv. 11 (2021) 27950–27964.

[17] N. Khiar-Fernández, J. Macicior, B. Marcos-Ramiro, S. Ortega-Gutiérrez, Chemistry for the identification of therapeutic targets: recent advances and future directions, Eur. J. Org. Chem. 2021 (2021) 1307–1320.

[18] S. Pan, A. Ding, Y. Li, Y. Sun, Y. Zhan, Z. Ye, N. Song, B. Peng, L. Li, W. Huang, H. Shao, Small-molecule probes from bench to bedside: advancing molecular analysis of drug-target interactions toward precision medicine, Chem. Soc. Rev. 52 (2023) 5706–5743.

[19] S. Lechner, R.R. Steimbach, L. Wang, M.L. Deline, Y.C. Chang, T. Fromme, M. Klingenspor, P. Matthias, A.K. Miller, G. Médard, B. Kuster, Chemoproteomic target deconvolution reveals Histone Deacetylases as targets of (*R*)-lipoic acid, Nat. Commun. 14 (2023) 3548.

[20] C.G. Parker, C.A. Kuttruff, A. Galmozzi, L. Jørgensen, C.H. Yeh, D.J. Hermanson, Y. Wang, M. Artola, S.J. McKerrall, C.M. Josyln, B. Nørremark, G. Dünstl, J. Felding, E. Saez, P.S. Baran, B.F. Cravatt, Chemical proteomics identifies SLC25A20 as a functional target of the Ingenol class of actinic keratosis drugs, ACS Cent. Sci. 3 (2017) 1276–1285.

[21] J. Tang, W. Li, T.Y. Chiu, F. Martínez-Peña, Z. Luo, C.T. Chong, Q. Wei, N. Gazaniga, T.J. West, Y.Y. See, L.L. Lairson, C.G. Parker, P.S. Baran, Synthesis of portimines reveals the basis of their anti-cancer activity, Nature 622 (2023) 507–513.

[22] A. Weigert Muñoz, K.M. Meighen-Berger, S.M. Hacker, M.J. Feige, S.A. Sieber, A chemical probe unravels the reactive proteome of health-associated catechols, Chem. Sci. 14 (2023) 8635–8643.

[23] Y.S. Cheng, T. Zhang, X. Ma, S. Pratuangtham, G.C. Zhang, A.A. Ondrus, A. Mafi, B. Lomenick, J.J. Jones, A.E. Ondrus, A proteome-wide map of 20(S)-hydroxycholesterol interactors in cell membranes, Nat. Chem. Biol. 17 (2021) 1271–1280.

[24] A.M. Gamo, J.A. Gonzalez-Vera, A. Rueda-Zubiaurre, D. Alonso, H. Vazquez-Villa, L. Martin-Couce, O. Palomares, J.A. Lopez, M. Martin-Fontecha, B. Benhamu, M.L. Lopez-Rodriguez, S. Ortega-Gutierrez, Chemoproteomic approach to explore the target profile of GPCR ligands: application to 5-$HT_{1A}$ and 5-$HT_6$ receptors, Chem. Eur J. 22 (2016) 1313–1321.

[25] C. Cui, B.G. Dwyer, C. Liu, D. Abegg, Z.J. Cai, D.G. Hoch, X. Yin, N. Qiu, J.Q. Liu, A. Adibekian, M. Dai, Total synthesis and target identification of the curcusone diterpenes, J. Am. Chem. Soc. 143 (2021) 4379–4386.

[26] X.W. Zhang, L. Li, M. Liao, D. Liu, A. Rehman, Y. Liu, Z.P. Liu, P.F. Tu, K.W. Zeng, Thermal proteome profiling strategy identifies CNPY3 as a cellular target of gambogic acid for inducing prostate cancer pyroptosis, J. Med. Chem. 67 (2024) 10005–10011.

[27] A.K. Bracken, C.E. Gekko, N.O. Suss, E.E. Lueders, Q. Cui, Q. Fu, A.C.W. Lui, E. T. Anderson, S. Zhang, M.E. Abbasov, Biomimetic synthesis and chemical proteomics reveal the mechanism of action and functional targets of phloroglucinol meroterpenoids, J. Am. Chem. Soc. 146 (2024) 2524–2548.

[28] T. Li, A. Wang, Y. Zhang, W. Chen, Y. Guo, X. Yuan, Y. Liu, Y. Geng, Chemoproteomic profiling of signaling metabolite fructose-1,6-bisphosphate interacting proteins in lving cells, J. Am. Chem. Soc. 146 (2024) 15155–15166.

[29] Z. Li, P. Hao, L. Li, C.Y. Tan, X. Cheng, G.Y. Chen, S.K. Sze, H.M. Shen, S.Q. Yao, Design and synthesis of minimalist terminal alkyne-containing diazirine photo-crosslinkers and their incorporation into kinase inhibitors for cell- and tissue-based proteome profiling, Angew. Chem. Int. Ed. 52 (2013) 8551–8556.

[30] D. Alonso, H. Vázquez-Villa, A.M. Gamo, M.F. Martínez-Esperón, M. Tortosa, A. Viso, R. Fernández de la Pradilla, E. Junquera, E. Aicart, M. Martín-Fontecha, B. Benhamú, M.L. López-Rodríguez, S. Ortega-Gutiérrez, Development of fluorescent ligands for the human 5-$HT_{1A}$ receptor, ACS Med. Chem. Lett. 1 (2010) 249–253.

[31] G. Hernandez-Torres, E. Enriquez-Palacios, M. Mecha, A. Feliu, A. Rueda-Zubiaurre, A. Angelina, L. Martin-Cruz, M. Martin-Fontecha, O. Palomares, C. Guaza, E. Pena-Cabrera, M.L. Lopez-Rodriguez, S. Ortega-Gutierrez, Development of a fluorescent bodipy probe for visualization of the serotonin 5-HT1A receptor in native cells of the immune system, Bioconjug. Chem. 29 (2018) 2021–2027.

[32] L. Martin-Couce, M. Martin-Fontecha, O. Palomares, L. Mestre, A. Cordomi, M. Hernangomez, S. Palma, L. Pardo, C. Guaza, M.L. Lopez-Rodriguez, S. Ortega-Gutierrez, Chemical probes for the recognition of cannabinoid receptors in native systems, Angew. Chem. Int. Ed. Engl. 51 (2012) 6896–6899.

[33] M. Martin-Fontecha, A. Angelina, B. Ruckert, A. Rueda-Zubiaurre, L. Martin-Cruz, W. van de Veen, M. Akdis, S. Ortega-Gutierrez, M.L. Lopez-Rodriguez, C.A. Akdis, O. Palomares, A fluorescent probe to unravel functional features of cannabinoid receptor CB1 in human blood and tonsil immune system cells, Bioconjug. Chem. 29 (2018) 382–389.

[34] L. Ma, J. Chen, X. Wang, X. Liang, Y. Luo, W. Zhu, T. Wang, M. Peng, S. Li, S. Jie, A. Peng, Y. Wei, L. Chen, Structural modification of honokiol, a biphenyl occurring in Magnolia officinalis: the evaluation of honokiol analogues as inhibitors of angiogenesis and for their cytotoxicity and structure-activity relationship, J. Med. Chem. 54 (2011) 6469–6481.

[35] H. Sung, J. Ferlay, R.L. Siegel, M. Laversanne, I. Soerjomataram, A. Jemal, F. Bray, Global cancer statistics 2020: GLOBOCAN estimates of incidence and mortality worldwide for 36 cancers in 185 countries, CA Cancer J. Clin. 71 (2021) 209–249.

[36] R.L. Siegel, K.D. Miller, N.S. Wagle, A. Jemal, Cancer statistics, CA Cancer J. Clin. 73 (2023) 17–48, 2023.

[37] G. Bianchini, C. De Angelis, L. Licata, L. Gianni, Treatment landscape of triple-negative breast cancer - expanded options, evolving needs, Nat. Rev. Clin. Oncol. 19 (2022) 91–113.

[38] M. Kobayashi, C. Salomon, J. Tapia, S.E. Illanes, M.D. Mitchell, G.E. Rice, Ovarian cancer cell invasiveness is associated with discordant exosomal sequestration of Let-7 miRNA and miR-200, J. Transl. Med. 12 (2014) 4.

[39] C.G. Parker, A. Galmozzi, Y. Wang, B.E. Correia, K. Sasaki, C.M. Joslyn, A.S. Kim, C.L. Cavallaro, R.M. Lawrence, S.R. Johnson, I. Narvaiza, E. Saez, B.F. Cravatt, Ligand and target discovery by fragment-based screening in human cells, Cell 168 (2017) 527–541.

[40] X. Chen, S. Wei, Y. Ji, X. Guo, F. Yang, Quantitative proteomics using SILAC: principles, applications, and developments, Proteomics 15 (2015) 3175–3192.

[41] I. Shapovalov, D. Harper, P.A. Greer, Calpain as a therapeutic target in cancer, Expert Opin. Ther. Targets 26 (2022) 217–231.

[42] Y.J. Chen, C.L. Wu, J.F. Liu, Y.C. Fong, S.F. Hsu, T.M. Li, Y.C. Su, S.H. Liu, C. H. Tang, Honokiol induces cell apoptosis in human chondrosarcoma cells through mitochondrial dysfunction and endoplasmic reticulum stress, Cancer Lett. 291 (2010) 20–30.

[43] J. Wang, Z. Yang, H. Bai, L. Zhao, J. Ji, Y. Bin, Y. Liu, S. Zhang, H. Hou, Q. Li, High-expressed ACAT2 predicted the poor prognosis of platinum-resistant epithelial ovarian cancer, Diagn. Pathol. 19 (2024) 7.

[44] J. Heng, Z. Li, L. Liu, Z. Zheng, Y. Zheng, X. Xu, L. Liao, H. Xu, H. Huang, E. Li, L. Xu, Acetyl-CoA acetyltransferase 2 confers radioresistance by inhibiting ferroptosis in esophageal squamous cell carcinoma, Int. J. Radiat. Oncol. Biol. Phys. 117 (2023) 966–978.
[45] M. Locatelli, C. Zoja, C. Zanchi, D. Corna, S. Villa, S. Bolognini, R. Novelli, L. Perico, G. Remuzzi, A. Benigni, P. Cassis, Manipulating sirtuin 3 pathway ameliorates renal damage in experimental diabetes, Sci. Rep. 10 (2020) 8418.
[46] X. Lv, F. Liu, Y. Shang, S.Z. Chen, Honokiol exhibits enhanced antitumor effects with chloroquine by inducing cell death and inhibiting autophagy in human non-small cell lung cancer cells, Oncol. Rep. 34 (2015) 1289–1300.
[47] R. Shetty, R. Noland, G. Nandi, C.K. Suzuki, Powering down the mitochondrial LonP1 protease: a novel strategy for anticancer therapeutics, Expert Opin. Ther. Targets 28 (2024) 9–15.
[48] Z. Hu, X. Bian, X. Liu, Y. Zhu, X. Zhang, S. Chen, K. Wang, Y. Wang, Honokiol protects brain against ischemia-reperfusion injury in rats through disrupting PSD95-nNOS interaction, Brain Res. 1491 (2013) 204–212.
[49] X. Wang, D. Xiao, C. Ma, L. Zhang, Q. Duan, X. Zheng, M. Mao, D. Zhu, Q. Li, The effect of honokiol on pulmonary artery endothelium cell autophagy mediated by cyclophilin A in hypoxic pulmonary arterial hypertension, J. Pharmaco. Sci. 139 (2019) 158–165.
[50] V.A. Kiesel, M.P. Sheeley, M.F. Coleman, E.K. Cotul, S.S. Donkin, S.D. Hursting, M.K. Wendt, D. Teegarden, Pyruvate carboxylase and cancer progression, Cancer Metab 9 (2021) 20.
[51] G.W. Sun, T.Y. Ding, M. Wang, C.L. Hu, J.J. Gu, J. Li, T. Qiu, Honokiol reduces mitochondrial dysfunction and inhibits apoptosis of nerve cells in rats with traumatic brain injury by activating the mitochondrial unfolded protein response, J. Mol. Neurosci. 72 (2022) 2464–2472.
[52] J. Yang, W. Wu, J. Wen, H. Ye, H. Luo, P. Bai, M. Tang, F. Wang, L. Zheng, S. Yang, W. Li, A. Peng, L. Yang, L. Wan, L. Chen, Liposomal honokiol induced lysosomal degradation of Hsp90 client proteins and protective autophagy in both gefitinib-sensitive and gefitinib-resistant NSCLC cells, Biomaterials 141 (2017) 188–198.
[53] H.C. Pan, D.W. Lai, K.H. Lan, C.C. Shen, S.M. Wu, C.S. Chiu, K.B. Wang, M. L. Sheu, Honokiol thwarts gastric tumor growth and peritoneal dissemination by inhibiting Tpl2 in an orthotopic model, Carcinogenesis 34 (2013) 2568–2579.
[54] Y.W. Kim, C. Kwon, J.L. Liu, S.H. Kim, S. Kim, Cancer association study of aminoacyl-tRNA synthetase signaling network in glioblastoma, PLoS One 7 (2012) e40960.
[55] Z.N. Li, Y. Luo, HSP90 inhibitors and cancer: prospects for use in targeted therapies, Oncol. Rep. 49 (2023) 6.
[56] C.J. Schmidlin, W. Tian, M. Dodson, E. Chapman, D.D. Zhang, FAM129B-dependent activation of NRF2 promotes an invasive phenotype in BRAF mutant melanoma cells, Mol. Carcinog. 60 (2021) 331–341.
[57] J. Piñero, J.M. Ramírez-Anguita, J. Saüch-Pitarch, F. Ronzano, E. Centeno, F. Sanz, L.I. Furlong, The DisGeNET knowledge platform for disease genomics: 2019 update, Nucleic Acids Res. 48 (2020) D845–d855.
[58] K. Banik, A.M. Ranaware, V. Deshpande, S.P. Nalawade, G. Padmavathi, D. Bordoloi, B.L. Sailo, M.K. Shanmugam, L. Fan, F. Arfuso, G. Sethi, A. B. Kunnumakkara, Honokiol for cancer therapeutics: a traditional medicine that can modulate multiple oncogenic targets, Pharmacol. Res. 144 (2019) 192–209.
[59] A. Rauf, S. Patel, M. Imran, A. Maalik, M.U. Arshad, F. Saeed, Y.N. Mabkhot, S. S. Al-Showiman, N. Ahmad, E. Elsharkawy, Honokiol: an anticancer lignan, Biomed. Pharmacother. 107 (2018) 555–562.
[60] E.J. Park, H.Y. Min, H.J. Chung, J.Y. Hong, Y.J. Kang, T.M. Hung, U.J. Youn, Y. S. Kim, K. Bae, S.S. Kang, S.K. Lee, Down-regulation of c-Src/EGFR-mediated signaling activation is involved in the honokiol-induced cell cycle arrest and apoptosis in MDA-MB-231 human breast cancer cells, Cancer Lett. 277 (2009) 133–140.
[61] S. Cheng, V. Castillo, I. Eliaz, D. Sliva, Honokiol suppresses metastasis of renal cell carcinoma by targeting KISS1/KISS1R signaling, Int. J. Oncol. 46 (2015) 2293–2298.
[62] S. Cheng, V. Castillo, M. Welty, I. Eliaz, D. Sliva, Honokiol inhibits migration of renal cell carcinoma through activation of RhoA/ROCK/MLC signaling pathway, Int. J. Oncol. 49 (2016) 1525–1530.
[63] W. Li, Q. Wang, Q. Su, D. Ma, C. An, L. Ma, H. Liang, Honokiol suppresses renal cancer cells' metastasis via dual-blocking epithelial-mesenchymal transition and cancer stem cell properties through modulating miR-141/ZEB2 signaling, Mol. Cells 37 (2014) 383–388.
[64] J. Jin, L. Bai, D. Wang, W. Ding, Z. Cao, P. Yan, Y. Li, L. Xi, Y. Wang, X. Zheng, H. Wei, C. Ding, Y. Wang, SIRT3-dependent delactylation of cyclin E2 prevents hepatocellular carcinoma growth, EMBO Rep. 24 (2023) e56052.
[65] Y.S. Lee, S. Jeong, K.Y. Kim, J.S. Yoon, S. Kim, K.S. Yoon, J. Ha, I. Kang, W. Choe, Honokiol inhibits hepatoma carcinoma cell migration through downregulated cyclophilin B expression, Biochem. Biophys. Res. Commun. 552 (2021) 44–51.
[66] H. Zhang, M. Huo, Y. Jia, A. Xu, KRT6B, a key mediator of notch signaling in honokiol-induced human hepatoma cell apoptosis, Int. J. Clin. Exp. Med. 8 (2015) 16880–16889.
[67] D.E. Johnson, B. Burtness, C.R. Leemans, V.W.Y. Lui, J.E. Bauman, J.R. Grandis, Head and neck squamous cell carcinoma, Nat. Rev. Dis. Primers 6 (2020) 92.
[68] X. Wang, J.J. Beitler, W. Huang, G. Chen, G. Qian, K. Magliocca, M.R. Patel, A. Y. Chen, J. Zhang, S. Nannapaneni, S. Kim, Z. Chen, X. Deng, N.F. Saba, Z. G. Chen, J.L. Arbiser, D.M. Shin, Honokiol radiosensitizes squamous cell carcinoma of the head and neck by downregulation of survivin, Clin. Cancer Res. 24 (2018) 858–869.
[69] T. Singh, N.A. Gupta, S. Xu, R. Prasad, S.E. Velu, S.K. Katiyar, Honokiol inhibits the growth of head and neck squamous cell carcinoma by targeting epidermal growth factor receptor, Oncotarget 6 (2015) 21268–21282.
[70] H. Mi, A. Muruganujan, J.T. Casagrande, P.D. Thomas, Large-scale gene function analysis with the PANTHER classification system, Nat. Protoc. 8 (2013) 1551–1566.
[71] I. Martínez-Reyes, N.S. Chandel, Cancer metabolism: looking forward, Nat. Rev. Cancer 21 (2021) 669–680.
[72] M. Demicco, X.Z. Liu, K. Leithner, S.M. Fendt, Metabolic heterogeneity in cancer, Nat. Metab. 6 (2024) 18–38.
[73] D. Hanahan, Hallmarks of cancer: new dimensions, Cancer Discov. 12 (2022) 31–46.
[74] S. Missiroli, M. Perrone, I. Genovese, P. Pinton, C. Giorgi, Cancer metabolism and mitochondria: finding novel mechanisms to fight tumours, EBioMedicine 59 (2020) 102943.
[75] W.X. Zong, J.D. Rabinowitz, E. White, Mitochondria and cancer, Mol. Cell 61 (2016) 667–676.
[76] P.E. Porporato, N. Filigheddu, J.M.B. Pedro, G. Kroemer, L. Galluzzi, Mitochondrial metabolism and cancer, Cell Res. 28 (2018) 265–280.
[77] P.J. Burke, Mitochondria, bioenergetics and apoptosis in cancer, Trends Cancer 3 (2017) 857–870.
[78] V.B. Pillai, S. Samant, N.R. Sundaresan, H. Raghuraman, G. Kim, M.Y. Bonner, J. L. Arbiser, D.I. Walker, D.P. Jones, D. Gius, M.P. Gupta, Honokiol blocks and reverses cardiac hypertrophy in mice by activating mitochondrial Sirt3, Nat. Commun. 6 (2015) 6656.
[79] X. Shi, T. Zhang, H. Lou, H. Song, C. Li, P. Fan, Anticancer effects of honokiol via mitochondrial dysfunction are strongly enhanced by the mitochondria-targeting carrier berberine, J. Med. Chem. 63 (2020) 11786–11800.
[80] J.X. Dong, G.Y. Zhao, Q.L. Yu, R. Li, L. Yuan, J. Chen, Y. Liu, Mitochondrial dysfunction induced by honokiol, J. Membr. Biol. 246 (2013) 375–381.
[81] J. Pan, Y. Lee, Y. Wang, M. You, Honokiol targets mitochondria to halt cancer progression and metastasis, Mol. Nutr. Food Res. 60 (2016) 1383–1395.
[82] Y. Song, X. Ma, M. Zhang, M. Wang, G. Wang, Y. Ye, W. Xia, Ezrin mediates invasion and metastasis in tumorigenesis: a review, Front. Cell Dev. Biol. 8 (2020) 588801.
[83] N.A. Kuburich, P. den Hollander, J.T. Pietz, S.A. Mani, Vimentin and cytokeratin: good alone, bad together, Semin. Cancer Biol. 86 (2022) 816–826.
[84] G. Dhiman, N. Srivastava, M. Goyal, E. Rakha, J. Lothion-Roy, N.P. Mongan, R. R. Miftakhova, S.F. Khaiboullina, A.A. Rizvanov, M. Baranwal, Metadherin: a therapeutic target in multiple cancers, Front. Oncol. 9 (2019) 349.
[85] D.B. Avtanski, A. Nagalingam, M.Y. Bonner, J.L. Arbiser, N.K. Saxena, D. Sharma, Honokiol inhibits epithelial-mesenchymal transition in breast cancer cells by targeting signal transducer and activator of transcription 3/Zeb1/E-cadherin axis, Mol. Oncol. 8 (2014) 565–580.
[86] W.D. Wang, Y. Shang, Y. Li, S.Z. Chen, Honokiol inhibits breast cancer cell metastasis by blocking EMT through modulation of Snail/Slug protein translation, Acta Pharmacol. Sin. 40 (2019) 1219–1227.
[87] D.W. Huang, B.T. Sherman, R.A. Lempicki, Systematic and integrative analysis of large gene lists using DAVID bioinformatics resources, Nat. Protoc. 4 (2009) 44–57.
[88] B.T. Sherman, M. Hao, J. Qiu, X. Jiao, M.W. Baseler, H.C. Lane, T. Imamichi, W. Chang, DAVID: a web server for functional enrichment analysis and functional annotation of gene lists (2021 update), Nucleic Acids Res. 50 (2022) W216–w221.
[89] A.R. Stram, R.M. Payne, Post-translational modifications in mitochondria: protein signaling in the powerhouse, Cell. Mol. Life Sci. 73 (2016) 4063–4073.
[90] V. Singh, M. Ram, R. Kumar, R. Prasad, B.K. Roy, K.K. Singh, Phosphorylation: implications in cancer, Protein J. 36 (2017) 1–6.
[91] V. Sica, J.M. Bravo-San Pedro, G. Stoll, G. Kroemer, Oxidative phosphorylation as a potential therapeutic target for cancer therapy, Int. J. Cancer 146 (2020) 10–17.
[92] J. Yang, C. Song, X. Zhan, The role of protein acetylation in carcinogenesis and targeted drug discovery, Front. Endocrinol. 13 (2022) 972312.
[93] N. Jiang, W. Li, S. Jiang, M. Xie, R. Liu, Acetylation in pathogenesis: revealing emerging mechanisms and therapeutic prospects, Biomed. Pharmacother. 167 (2023) 115519.
[94] N.R. Jayakumari, R.S. Rajendran, A. Sivasailam, S.T. Parambil, A.C. Reghuvaran, H.V. Sreelatha, S. Gopala, Honokiol regulates mitochondrial substrate utilization and cellular fatty acid metabolism in diabetic mice heart, Eur. J. Pharmacol. 896 (2021) 173918.
[95] D. Mellacheruvu, Z. Wright, A.L. Couzens, J.P. Lambert, N.A. St-Denis, T. Li, Y. V. Miteva, S. Hauri, M.E. Sardiu, T.Y. Low, V.A. Halim, R.D. Bagshaw, N. C. Hubner, A. Al-Hakim, A. Bouchard, D. Faubert, D. Fermin, W.H. Dunham, M. Goudreault, Z.Y. Lin, B.G. Badillo, T. Pawson, D. Durocher, B. Coulombe, R. Aebersold, G. Superti-Furga, J. Colinge, A.J. Heck, H. Choi, M. Gstaiger, S. Mohammed, I.M. Cristea, K.L. Bennett, M.P. Washburn, B. Raught, R.M. Ewing, A.C. Gingras, A.I. Nesvizhskii, The CRAPome: a contaminant repository for affinity purification-mass spectrometry data, Nat. Methods 10 (2013) 730–736.
[96] R. Jafari, H. Almqvist, H. Axelsson, M. Ignatushchenko, T. Lundbäck, P. Nordlund, D. Martinez Molina, The cellular thermal shift assay for evaluating drug target interactions in cells, Nat. Protoc. 9 (2014) 2100–2122.
[97] S. Sriramulu, X.F. Sun, S. Malayaperumal, H. Ganesan, H. Zhang, M. Ramachandran, A. Banerjee, S. Pathak, Emerging role and clinicopathological significance of AEG-1 in different cancer types: a concise review, Cells 10 (2021) 1497.
[98] R. Lin, S. Elf, C. Shan, H.B. Kang, Q. Ji, L. Zhou, T. Hitosugi, L. Zhang, S. Zhang, J. H. Seo, J. Xie, M. Tucker, T.L. Gu, J. Sudderth, L. Jiang, M. Mitsche, R.

J. DeBerardinis, S. Wu, Y. Li, H. Mao, P.R. Chen, D. Wang, G.Z. Chen, S. J. Hurwitz, S. Lonial, M.L. Arellano, H.J. Khoury, F.R. Khuri, B.H. Lee, Q. Lei, D. J. Brat, K. Ye, T.J. Boggon, C. He, S. Kang, J. Fan, J. Chen, 6-Phosphogluconate dehydrogenase links oxidative PPP, lipogenesis and tumour growth by inhibiting LKB1-AMPK signalling, Nat. Cell Biol. 17 (2015) 1484–1496.

[99] H. Yamakoshi, K. Dodo, A. Palonpon, J. Ando, K. Fujita, S. Kawata, M. Sodeoka, Alkyne-tag Raman imaging for visualization of mobile small molecules in live cells, J. Am. Chem. Soc. 134 (2012) 20681–20689.

[100] A.E. Speers, B.F. Cravatt, Profiling enzyme activities in vivo using click chemistry methods, Chem. Biol. 11 (2004) 535–546.

[101] N.I. Marin-Ramos, M. Balabasquer, F.J. Ortega-Nogales, I.R. Torrecillas, A. Gil-Ordonez, B. Marcos-Ramiro, P. Aguilar-Garrido, I. Cushman, A. Romero, F. J. Medrano, C. Gajate, F. Mollinedo, M.R. Philips, M. Campillo, M. Gallardo, M. Martin-Fontecha, M.L. Lopez-Rodriguez, S. Ortega-Gutierrez, A potent isoprenylcysteine carboxylmethyltransferase (ICMT) inhibitor improves survival in Ras-driven acute myeloid leukemia, J. Med. Chem. 62 (2019) 6035–6046.

[102] M.P. Washburn, D. Wolters, J.R. Yates, 3rd. Large-scale analysis of the yeast proteome by multidimensional protein identification technology, Nat. Biotechnol. 19 (2001) 242–247.

[103] E. Weerapana, C. Wang, G.M. Simon, F. Richter, S. Khare, M.B. Dillon, D. A. Bachovchin, K. Mowen, D. Baker, B.F. Cravatt, Quantitative reactivity profiling predicts functional cysteines in proteomes, Nature 468 (2010) 790–795.

[104] B. Marcos-Ramiro, A. Gil-Ordóñez, N.I. Marín-Ramos, F.J. Ortega-Nogales, M. Balabasquer, P. Gonzalo, N. Khiar-Fernández, L. Rolas, A. Barkaway, S. Nourshargh, V. Andrés, M. Martín-Fontecha, M.L. López-Rodríguez, S. Ortega-Gutiérrez, Isoprenylcysteine carboxylmethyltransferase-based therapy for hutchinson-gilford progeria syndrome, ACS Cent. Sci. 7 (2021) 1300–1310.

[105] J. Macicior, D. Fernández, S. Ortega-Gutiérrez, A new fluorescent probe for the visualization of progerin, Bioorg. Chem. 142 (2024) 106967.